









**Anura3D MPM Research Community**

# Anura3D MPM Software

## Scientific Manual

Version: 2021 – Centro
29 April 2021

**Anura3D MPM Software, Scientific Manual**

*With the contributions of:*

| | |
|---|---|
| Francesca Ceccato | Università degli Studi di Padova, Italy |
| James Fern | Amberg Engineering Ltd / EPFL, Switzerland |
| Mario Martinelli | Deltares Delft, The Netherlands |
| Alexander Rohe | Deltares Delft, The Netherlands |
| Alba Yerro | VirginiaTech, United States |

Contributors are listed in alphabetical order. Many people contributed to the creation of this tutorial. If you feel that you are one of them but your name does not appear in this list, please contact us.

**Published and printed by:**
Anura3D MPM Research Community
c/o Stichting Deltares
Boussinesqweg 1
2629 HV Delft (The Netherlands)

**Contact and information:**
e-mail: info@Anura3D.com
web: www.Anura3D.com

# Contents

**Anura3D MPM Research Community**
c/o Stichting Deltares
Boussinesqweg 1
2629 HV Delft (The Netherlands)

**Contact and information**
e-mail: info@Anura3D.com
web: www.Anura3D.com

# 1 Introduction

This manual presents the the theories and numerical methods used in Anura3D. It contains a chapter on the mathematical formulation and the dynamic-explicit material point formulation of the 1-phase solid, 1-phase liquid and 2-phase mixture. The boundary conditions and advanced concepts used in the current version of Anura3D are also described in two separated sections. Lastly, a dedicated chapter on material models available in this code is also added for completeness. Additional scientific material can be found in the *Publications* section of the website.

# 2 General Framework

The material point method (MPM) was initially developed by Harlow [1] in Los Alamos National Laboratory. The basis of that method, called initially Particle-In-Cell method (PIC), was to represent fluid flow by a set of material points moving through a background fixed mesh. Later, in 1994 in the New Mexico University, Sulsky and Schreyer [2–4] extended the approach for modelling problems of solid mechanics, where basically the equation of dynamic momentum balance is discretized.

MPM is considered as a method in between the particle-based methods and the Finite Element Method (FEM). This is because it discretizes the media in two different frames. First, the continuum is divided into a set of material points (MPs). Each material point represents a portion of the domain and the mass of such sub-domain, assumed to be fixed during all the calculation (to ensure mass conservation). In the classical MPM, it is considered to be concentrated at the corresponding material point. Other quantities such as velocities, strains and stresses, are also initialized and carried by the MPs. Each material point moves attached with the deformations of the body and this provides the Lagrangian description of the media.

The second frame is a computational mesh. It is the same as the one used in the conventional FEM and it is built to cover the full domain of the problem. The discrete governing equations are solved at the nodes of the computational mesh. The variables required to solve the equations in the mesh at any step of the analysis are transferred from the material points to the nodes of the mesh by using mapping functions. For instance, the typical linear shape functions used in the FEM. Boundary conditions can be imposed at the mesh nodes or at the material points and the governing equations are solved by using an incremental scheme. Then the quantities carried by the material points are updated through the interpolation of the mesh results, using the same mapping functions. The information associated with the mesh is not required for the next step of the analysis; therefore it can be discarded avoiding any mesh distortion.

Fig. 2.1 is a typical problem setup. The material domain is represented by a set of material points. The computational mesh covers all the computational domain.

At the beginning of each time increment, the discretized governing equations are defined by mapping information from the MPs to the computational nodes of the mesh by means of the interpolation functions (Fig. 2.2a). The governing equations of motion are solved for the primary unknown variables, e.g the nodal accelerations (Fig. 2.2b). This nodal values are used to update acceleration, velocity and position of MPs, as well as to compute strains and stresses at the MPs (Fig. 2.2c). No permanent information is stored in the mesh, thus it can be freely redefined at the end of the time step, but commonly it is kept fix. The assignment of MPs to finite elements is updated after mesh adjustment (Fig. 2.2d).

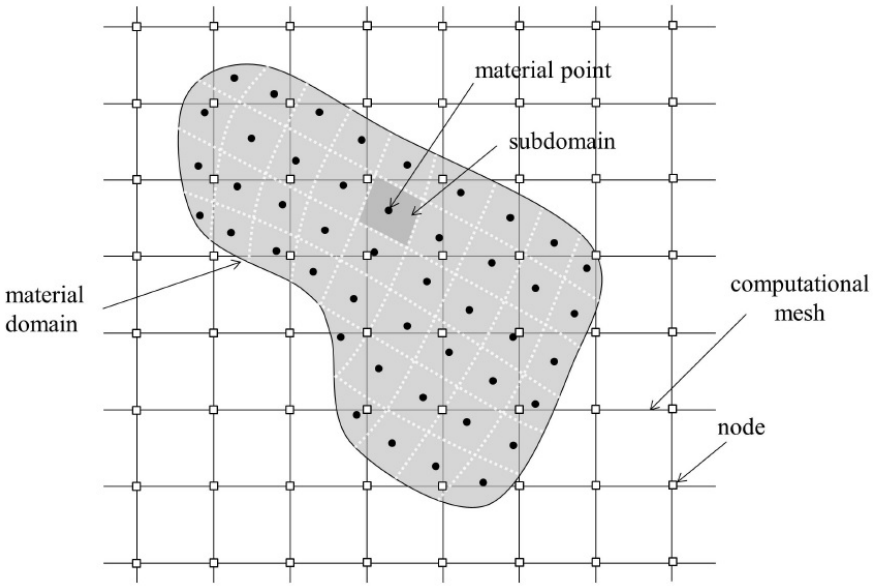


***Figure 2.1:*** *Space discretisation. Nodes of the computational mesh and material points, after [5]*

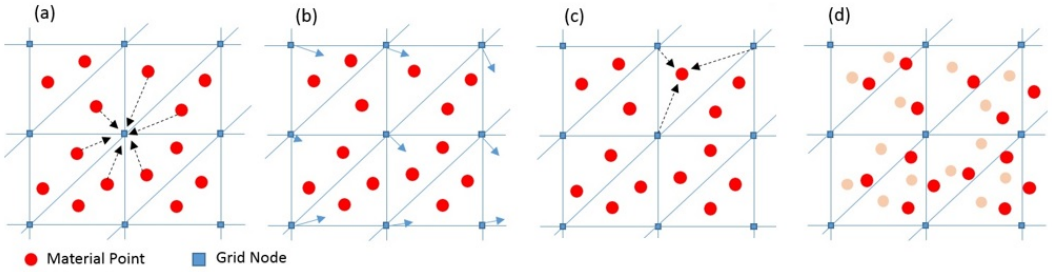


***Figure 2.2:*** *Computation scheme of MPM: (a) map information from MPs to grid nodes; (b) solve governing equations of motion at the nodes; (c) update MP information; (c) update MP position and housekeeping*

# 3 Mathematical formulation

## 3.1 Introduction

This chapter presents the basic equations for the dynamic equilibrium of the solid body and the porous media within the framework of continuum mechanics. The variational form, or weak form, of the corresponding partial differential equations is also developed.

## 3.2 1-phase-solid analysis with material point method

The MPM formulation for mechanical problems (1-phase MPM formulation) is presented in this Section. It is based on [3], in which only a single phase is considered. Because the MPM can be viewed as an extension of the FEM procedure, is important to note that they have much in common. For instance, the weak form of the governing equations as well as the final system of equations posed at the nodes of the computational mesh are identical in both schemes. The most distinguishing feature between them is the calculation of the numerical integrations over the volume of a finite element. Meanwhile in FEM the integrations are carried out using Gaussian quadrature, in MPM they are calculated based on the material points.

Three-dimensional domains are considered in this Chapter. Vectors and tensors are identified with bold type.

### 3.2.1 Governing equations

From a mathematical point of view, the continuum can be described by a set of differential governing equations. This includes conservation of mass, conservation of momentum, balance of energy and the corresponding boundary conditions. Furthermore, constitutive equations such as stress-strain relationship, which are characteristic of the material forming the continuum, are needed. It is worth noticing that thermal effects are very small hence they have been neglected in all the document.

#### 3.2.1.1 Mass conservation

The conservation of mass of the solid phase in Lagrangian form is written with the following partial differential equation:

$$\frac{\mathrm{d}}{\mathrm{d}t}\rho + \rho\nabla\cdot\mathbf{v}_S = 0 \tag{3.1}$$

in which $\mathbf{v}$ is the velocity vector of the solid phase. One of the features of the MPM formulation for a 1-phase material is that the mass of each material point $m_{MP}$ remains constant during all calculation. This fact implies that mass conservation is automatically satisfied.

#### 3.2.1.2 Momentum balance equation

The momentum conservation of the continuum can be written with the differential Eq. 3.2. A dynamic formulation is considered, which means that the acceleration term is taken into account.

$$\rho\frac{\mathrm{d}\mathbf{v}_S}{\mathrm{d}t} = \nabla\cdot\boldsymbol{\sigma}_S + \rho\mathbf{b} \tag{3.2}$$

The density of the continuum is represented by $\rho$, $\frac{d\mathbf{v}_S}{dt}$ is the acceleration, $\boldsymbol{\sigma}_S$ is the Cauchy stress tensor, and **b** is the body force vector.

Two kind of boundary conditions are defined: prescribed traction (Eq. 3.3) and prescribed displacements (Eq. 3.4). Each one is applied on the corresponding domain, $\partial\Omega^{\boldsymbol{\sigma}}$ and $\partial\Omega^{\mathbf{u}}$ respectively,

$$\boldsymbol{\sigma}_S(\mathbf{x}, t) \cdot \mathbf{n} = \widehat{\mathbf{t}}_S(t) \tag{3.3}$$

$$\mathbf{u}_S(\mathbf{x}, t) = \widehat{\mathbf{u}}_S(t) \tag{3.4}$$

where $\boldsymbol{\sigma}_S(\mathbf{x}, t)$ is the stress tensor, **n** is the outward unit normal vector of the free surface, and $\widehat{\mathbf{t}}_S(t)$ is the surface traction vector. **x** is the position vector, $\mathbf{u}_S$ is the displacement vector, and t is time.

### 3.2.2 Weak form

The conservation of the momentum (Eq. 3.2) is a key equation in continuum mechanics, representing the equation of motion of the continuum. To discretize this equation, its strong form has to be transformed into the weak form or the well-known virtual work equation. The momentum equation is now multiplied by a test function or a virtual velocity $\delta v$ and is integrated over the current domain $\Omega$ occupied by the continuum, i.e.,

$$\int_\Omega \delta\mathbf{v}_S \rho \frac{d\mathbf{v}_S}{dt} d\Omega = \int_\Omega \delta\mathbf{v}_S (\nabla \cdot \boldsymbol{\sigma}_S) d\Omega + \int_\Omega \delta\mathbf{v}_S \rho \mathbf{g} d\Omega \tag{3.5}$$

with $\delta\mathbf{v} = 0$ on $\partial\Omega_u$.

The first term on the right-hand side of Eq. (3.5) can be expressed as

$$\int_\Omega \delta\mathbf{v}_S (\nabla \cdot \boldsymbol{\sigma})_S \, d\Omega = \int_\Omega (\nabla \cdot \delta\mathbf{v}_S \boldsymbol{\sigma}_S) \, d\Omega - \int_\Omega (\nabla \cdot \delta\mathbf{v}_S) \boldsymbol{\sigma}_S \, d\Omega \tag{3.6}$$

Using Gauss theorem, also called divergence theorem, the first term on the right-hand side of Eq. (3.6) can be written as

$$\int_\Omega (\nabla \cdot \delta\mathbf{v}_S \boldsymbol{\sigma}_S) \, d\Omega = \int_{\partial\Omega_\sigma} \delta\mathbf{v}_S \, \boldsymbol{\tau}_S \, d\partial\Omega \tag{3.7}$$

Substituting all previous terms in Eq. (3.5), it follows

$$\int_\Omega \delta\mathbf{v}_S \rho \frac{d\mathbf{v}_S}{dt} d\Omega = \int_{\partial\Omega_\sigma} \delta\mathbf{v}_S \, \boldsymbol{\tau}_S \, d\partial\Omega - \int_\Omega (\nabla \cdot \delta\mathbf{v}_S) \boldsymbol{\sigma}_S \, d\Omega + \int_\Omega \delta\mathbf{v}_S \rho \mathbf{g} d\Omega \tag{3.8}$$

which will be used then in the formulation of the discrete equations.

## 3.3 1-phase-liquid analysis with material point method

### 3.3.1 Governing equations

In this section, the conservation equations of mass and linear momentum are written with respect to the liquid phase.

#### 3.3.1.1 Mass conservation

The conservation of mass of the liquid phase in a lagrangian form is written as follows:

$$\frac{d\rho_L}{dt} + \rho_L \nabla \cdot \mathbf{v}_L = 0 \tag{3.9}$$

in which $\mathbf{v_L}$ is the velocity vector of the liquid phase. As written for the solid phase, one of the features of the MPM formulation is that the mass of each material point $m_{MP}$ remains constant during all calculation. This fact implies that mass conservation is automatically satisfied.

#### 3.3.1.2 Momentum balance equation

The momentum conservation of the continuum can be written with the differential Eq. 3.10. A dynamic formulation is considered, which means that the acceleration term is taken into account.

$$\rho_L \frac{d\mathbf{v}_L}{dt} = \nabla \cdot \boldsymbol{\sigma}_L + \rho_L \mathbf{b} \tag{3.10}$$

The liquid density of the continuum is represented by $\rho_L$, $\mathbf{v}_L$ is the velocity, $\boldsymbol{\sigma_L}$ is the Cauchy stress tensor, and $\mathbf{b}$ is the body force vector.

Two kind of boundary conditions are defined: prescribed traction (Eq. 3.11) and prescribed displacements (Eq. 3.12, Fig. 3.1). Each one is applied on the corresponding domain, $\partial\Omega^{\boldsymbol{\sigma}}$ and $\partial\Omega^{\mathbf{u}}$ respectively. The boundary condition along $\partial\Omega^{\boldsymbol{\sigma}}$ is defined as follows:

$$\boldsymbol{\sigma}_L(\mathbf{x}, t) \cdot \mathbf{n} = \widehat{\mathbf{t}}(\mathbf{x}, t) \tag{3.11}$$

where $\boldsymbol{\sigma}_L(\mathbf{x}, t)$ is the stress tensor, $\mathbf{n}$ is the outward unit normal vector of the free surface and $\widehat{\mathbf{t}}(\mathbf{x}, t)$ is the surface traction vector. The boundary condition along $\partial\Omega^{\mathbf{u}}$ is defined as follows:

$$\mathbf{u}(\mathbf{x}, t) = \widehat{\mathbf{u}}(t) \tag{3.12}$$

$\mathbf{x}$ is the position vector, $\widehat{\mathbf{u}}$ is the displacement vector and t is time.

The boundary between liquid and gas phase is the *free surface* and is modelled as a boundary condition on $\partial\Omega_\sigma$. In case of zero surface tension and setting the atmospheric pressure to zero, such a boundary condition is set as $\widehat{\mathbf{t}}(\mathbf{x}, t) = p(\mathbf{x}, t) = 0$.

### 3.3.2 Weak form

The discretization of the equation of conservation of linear momentum for pure liquid is written as follows. The strong form of the equation is transformed into the weak form or the well-known virtual work equation. The momentum equation is now multiplied by a test function or a virtual velocity $\delta v$ and is integrated over the current domain $\Omega$ occupied by the continuum, i.e.,

$$\int_\Omega \delta\mathbf{v}_L \rho \frac{d\mathbf{v}_L}{dt} d\Omega = \int_\Omega \delta\mathbf{v}_L (\nabla \cdot \boldsymbol{\sigma}_L) d\Omega + \int_\Omega \delta\mathbf{v}_L \rho \mathbf{g} d\Omega \tag{3.13}$$

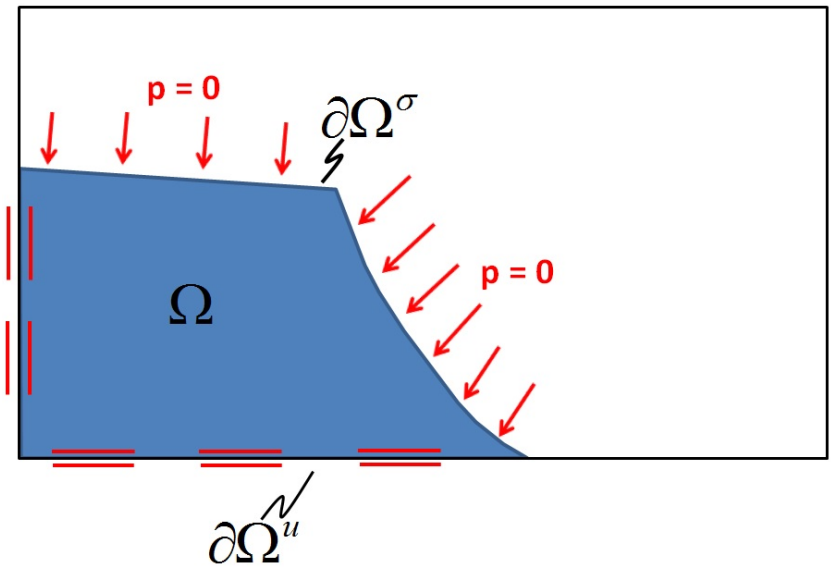


***Figure 3.1:*** *Water column collapse. Boundary conditions: displacements on* $\partial\Omega^{u}$ *and pressure on* $\partial\Omega^{\sigma}$.

with $\delta v = 0$ on $\partial\Omega_u$.

The first term on the right-hand side of Eq. (3.13) can be expressed as

$$\int_{\Omega} \delta \mathbf{v}_L (\nabla \cdot \boldsymbol{\sigma}_L)\, d\Omega = \int_{\Omega} (\nabla \cdot \delta \mathbf{v}_L \boldsymbol{\sigma}_L)\, d\Omega - \int_{\Omega} (\nabla \cdot \delta \mathbf{v}_L) \boldsymbol{\sigma}_L\, d\Omega \tag{3.14}$$

Using Gauss theorem, also called divergence theorem, the first term on the right-hand side of Eq. (3.14) can be written as

$$\int_{\Omega} (\nabla \cdot \delta \mathbf{v}_L \boldsymbol{\sigma}_L)\, d\Omega = \int_{\partial\Omega_\sigma} \delta \mathbf{v}_L\, \boldsymbol{\tau}_L\, d\partial\Omega \tag{3.15}$$

Substituting all previous terms in Eq. (3.5), it follows

$$\int_{\Omega} \delta \mathbf{v}_L \rho \frac{d\mathbf{v}_L}{dt} d\Omega = \int_{\partial\Omega_\sigma} \delta \mathbf{v}_L\, \boldsymbol{\tau}_L\, d\partial\Omega - \int_{\Omega} (\nabla \cdot \delta \mathbf{v}_L) \boldsymbol{\sigma}_L\, d\Omega + \int_{\Omega} \delta \mathbf{v}_L \rho \mathbf{g} d\Omega \tag{3.16}$$

which will be used then in the formulation of the discrete equations.

## 3.4 2-phase-coupled with single material point

### 3.4.1 Governing equations

This section is devoted to the presentation of the governing equations that are implemented in Anura3Dfor the solution of coupled dynamic, two-phase problems. It's worth mentioning that several coupled two-phase formulation have been discussed in the literature since the pioneering work by Terzaghi and Biot. The reader can refer to the work by Zienkiewicz and co-workers ([6], [7] and [8]) for a comprehensive discussion on this topic.

With the formulation used in Anura3D, the equilibrium equations are solved for the accelerations of pore liquid and soil skeleton as the primary unknown variables. This formulation proved to be able to capture the physical response of saturated soil under dynamic as well as static loading [9]. The governing equations are the mass conservation, and the momentum conservation of each phase and the mixture.

#### 3.4.1.1 Mass conservation

The mass conservation of the solid phase is expressed as:

$$\frac{d}{dt}[(1-n)\rho_S] + (1-n)\rho_S \nabla \cdot \mathbf{v}_S = 0 \tag{3.17}$$

in which $\mathbf{v}_S$ is the velocity vector of the solid phase and n is the porosity of the solid skeleton.

On denoting the components of the vector of the (true) velocity of the liquid phase as $\mathbf{v}_L$, the conservation of mass of this phase can be written as:

$$\frac{d(n\rho_L)}{dt} + n\rho_L \nabla \cdot \mathbf{v}_L = 0 \tag{3.18}$$

When considering incompressible solid grains and disregarding the spatial variations in densities and porosity, one can reduce the expression for the conservation of mass of the solid and liquid phases to

$$-\frac{dn}{dt} + (1-n)\nabla \cdot \mathbf{v}_S = 0 \tag{3.19}$$

and

$$\rho_L \frac{dn}{dt} + n\frac{d\rho_L}{dt} + n\rho_L \nabla \cdot \mathbf{v}_L = 0 \tag{3.20}$$

respectively. Substituting Equation 3.19 into Equation 3.20 allows to eliminate the term $\frac{dn}{dt}$. Hence,

$$(1-n)\nabla \cdot \mathbf{v}_S + \frac{n}{\rho_L}\frac{d\rho_L}{dt} + n\nabla \cdot \mathbf{v}_L = 0 \tag{3.21}$$

The liquid is considered as weakly compressible material. The effective volumetric strain $\bar{\varepsilon}_L$ in the liquid is defined as

$$\frac{d\bar{\varepsilon}_L}{dt} = -\frac{1}{\rho_L}\frac{d\rho_L}{dt} \tag{3.22}$$

Substituting Equation 3.22 into Equation 3.21 and rearranging terms yields:

$$\frac{d\bar{\varepsilon}_L}{dt} = \frac{1}{n}\left[(1-n)\nabla \cdot \mathbf{v}_S + n\nabla \cdot \mathbf{v}_L\right] \tag{3.23}$$

Equation 3.23 represents the conservation of mass of the saturated soil. It is also known as storage equation.

#### 3.4.1.2 Conservation of momentum

The conservation of momentum of the solid phase can be expressed as

$$(1-n)\rho_S\frac{d\mathbf{v}_S}{dt} - \nabla\cdot\boldsymbol{\sigma}' - (1-n)\nabla p_L - (1-n)\rho_S\mathbf{g} - \frac{n^2\rho_L g}{k}(\mathbf{v}_L - \mathbf{v}_S) = 0 \tag{3.24}$$

where k is the isotropic Darcy permeability. It can be expressed in terms of the intrinsic permeability $\kappa$ and the dynamic viscosity of the liquid $\mu_d$ as:

$$k = \kappa\frac{\rho_L g}{\mu_d} \tag{3.25}$$

The conservation of momentum of the liquid phase is written as:

$$n\rho_L\frac{d\mathbf{v}_L}{dt} - n\nabla p_L - n\rho_L\mathbf{g} + \frac{n^2\rho_L g}{k}(\mathbf{v}_L - \mathbf{v}_S) = 0 \tag{3.26}$$

the term $(\mathbf{v}_L - \mathbf{v}_S)$ represents the relative velocity of the liquid respect to the solid.

Adding the momentum of the solid phase (Eq. 3.24) to the momentum of the liquid phase (Eq. 3.26), the momentum conservation for the mixture can be written as:

$$(1-n)\rho_S\frac{d\mathbf{v}_L}{dt} + n\rho_L\frac{d\mathbf{v}_L}{dt} = \nabla\cdot\boldsymbol{\sigma} + \rho_{sat}\mathbf{g} \tag{3.27}$$

Summarizing, the two-phase problem is described by two momentum equations, i.e. 3.26 for the liquid and 3.27 for the mixture, the storage Eq. 3.23, and the constitutive equation for the soil skeleton. These equations are derived neglecting the spatial variation of densities and porosity, assuming incompressible soil grains, and assuming the validity of the Darcy's law.

#### 3.4.1.3 Boundary conditions

The proposed formulation requires that the boundary of the domain is the union of the following components

$$\partial\Omega = \partial\Omega_u \cup \partial\Omega_\sigma = \partial\Omega_{v_L} \cup \partial\Omega_p \tag{3.28}$$

where $\partial\Omega_{v_L}$ and $\partial\Omega_p$ are the prescribed velocity and prescribed pressure boundaries of the liquid phase, respectively, whereas $\partial\Omega_u$ is the prescribed displacement (velocity) boundary of the solid phase and $\partial\Omega_\sigma$ is the prescribed total stress boundary.

The following conditions should also be satisfied at the boundary

$$\partial\Omega_u \cap \partial\Omega_\sigma = \emptyset \quad \text{and} \quad \partial\Omega_{v_L} \cap \partial\Omega_p = \emptyset \tag{3.29}$$

### 3.4.2 Weak form

Before the discretization, the strong form of the governing equations has to be transformed in the weak form. This is achieved by multiplying Equations 3.26 and 3.27 by weighting function $\mathbf{t}$ and integrating over the current domain $\Omega$:

$$\int_\Omega \delta\mathbf{t}\rho_L\frac{d\mathbf{v}_L}{dt}d\Omega = \int_\Omega \delta\mathbf{t}\nabla p_L d\Omega + \int_\Omega \delta\mathbf{t}\rho_L\mathbf{g}d\Omega - \int_\Omega \delta\mathbf{t}\frac{n\rho_L g}{k}(\mathbf{v}_L - \mathbf{v}_S)d\Omega \tag{3.30}$$

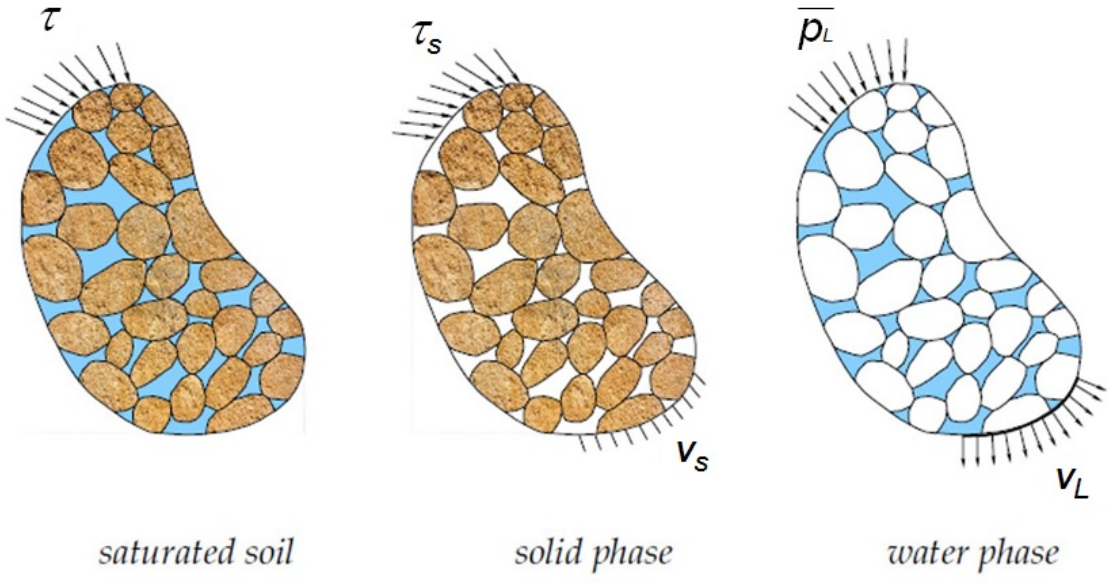


***Figure 3.2:*** *Displacement and traction boundary conditions for two phase problem (Al-Kafaji 2013) [10].*

$$\int_\Omega \delta \mathbf{t}(1-n)\rho_S \frac{d\mathbf{v}_S}{dt} d\Omega = \int_\Omega \delta \mathbf{t} \nabla \cdot \boldsymbol{\sigma}' d\Omega + \int_\Omega \delta \mathbf{t} \rho_{sat} \mathbf{g} d\Omega - \int_\Omega \delta \mathbf{t} n \rho_L \frac{d\mathbf{v}_L}{dt} d\Omega \tag{3.31}$$

Applying the divergence theorem and the traction boundary conditions, the final weak forms are:

$$\int_\Omega \delta \mathbf{t} \rho_L \frac{d\mathbf{v}_L}{dt} d\Omega = \int_{\partial\Omega_p} \delta \mathbf{t} \bar{p}_L dS - \int_\Omega \nabla \delta \mathbf{t} p_L d\Omega + \int_\Omega \delta \mathbf{t} \rho_L \mathbf{g} d\Omega - \int_\Omega \delta \mathbf{t} \frac{n \rho_L g}{k} (\mathbf{v}_L - \mathbf{v}_S) d\Omega \tag{3.32}$$

$$\int_\Omega \delta \mathbf{t}(1-n)\rho_S \frac{d\mathbf{v}_S}{dt} d\Omega = + \int_{\partial\Omega_\sigma} \delta \mathbf{t} \boldsymbol{\tau} dS - \int_\Omega \nabla \delta \mathbf{t} \boldsymbol{\sigma} d\Omega + \int_\Omega \delta \mathbf{t} \rho_{sat} \mathbf{g} d\Omega - \int_\Omega \delta \mathbf{t} n \rho_L \frac{d\mathbf{v}_L}{dt} d\Omega \tag{3.33}$$

The left-hand side terms in Equations 3.32 and 3.33 represent the inertia. In the right-hand side, the first terms represent the external load applied at the boundary, the second terms represent the internal force, and the third terms represent the gravity load. The last term in Equation 3.32 is the drag force. The last term in Equation 3.33 is the liquid inertia, where the porosity is taken into account.

# 4 Explicit-Dynamic Formulation

## 4.1 Introduction

This chapter presents the computation scheme adopted in the dynamic explicit implementation of Anura3D. It explains how the system of solving equations of the problem is assembled within the MPM framework and the main computational steps of the MPM solution procedure. A global calculation scheme is also provided for each of the computational cases: 1-phase-solid, 1-phase-liquid and 2-phase-mixture.

## 4.2 Notations and variables

The strain and stress tensors can be represented in vector form, taking advantage of the symmetry of the strain and stress tensors

$$\boldsymbol{\varepsilon}(\mathbf{x}, t) = [\varepsilon_{11}\ \varepsilon_{22}\ \varepsilon_{33}\ 2\varepsilon_{12}\ 2\varepsilon_{23}\ 2\varepsilon_{31}]^T \tag{4.1}$$

$$\boldsymbol{\sigma}(\mathbf{x}, t) = [\sigma_{11}\ \sigma_{22}\ \sigma_{33}\ \sigma_{12}\ \sigma_{23}\ \sigma_{31}]^T \tag{4.2}$$

where the first three terms in the vectors ($\sigma_{ij}$ and $\varepsilon_{ij}$ with i = j) are the normal components along the axis $x_i$ of the coordinate system and the other three represent the shear terms acting on the $x_i x_j$ planes. This way to represent the stress and strain is known in the literature as *Voigt* notation and is very useful as it reduces the order of the symmetric tensors.

It should be realized that the representation of the strain is different from stress in Voigt notation. The last three terms of the strain vector are represented by $\gamma_{ij} = 2\varepsilon_{ij}$. The reason for this is to ensure that energy is preserved and that different expressions of energy using tensors or vectors are equal,i.e.

$$\varepsilon_{ij}\sigma_{ij} = \varepsilon^T\boldsymbol{\sigma} \tag{4.3}$$

## 4.3 1-phase-solid analysis with material point method

### 4.3.1 Discretized momentum balance equation

The weak form of the linear momentum equation over the domain $\Omega$ is given by

$$\int_\Omega \delta\mathbf{v}\rho\frac{d\mathbf{v}}{dt}d\Omega = \int_{\partial\Omega_\sigma} \delta\mathbf{v}\ \boldsymbol{\tau}\ d\partial\Omega - \int_\Omega (\nabla\cdot\delta\mathbf{v})\boldsymbol{\sigma}\ d\Omega + \int_\Omega \delta\mathbf{v}\rho\mathbf{g}d\Omega \tag{4.4}$$

The domain $\Omega$ is decomposed into finite subdomains $\Omega_{el}$ called finite elements. The union of these subdomains comprises the total domain, $\Omega = \cup_{el=1}^{nelm}\Omega_{el}$, where nelm denotes the total number of finite elements in the mesh. Each element is jointed with its surrounding elements by points called nodes. The state variable is assumed to have pre-defined interpolation functions within the element and the solution is then obtained at the nodes. Hence, the equilibrium is satisfied at the nodes. It is usual in the finite element method to use matrix notations in the discretization of the virtual work equation.

In finite element method, the discrete form is obtained by approximating the displacement and

eventually the velocity and acceleration as

$$\begin{aligned}\mathbf{u}(\mathbf{x},t) &\approx \bar{\mathbf{N}}(\mathbf{x})\hat{\mathbf{u}}(t)\\ \mathbf{v}(\mathbf{x},t) &\approx \bar{\mathbf{N}}(\mathbf{x})\hat{\mathbf{v}}(t)\\ \mathbf{a}(\mathbf{x},t) &\approx \bar{\mathbf{N}}(\mathbf{x})\hat{\mathbf{a}}(t)\end{aligned} \tag{4.5}$$

respectively. The corresponding virtual quantities are approximated the same way, for instance,

$$\delta\mathbf{u}(\mathbf{x},t) \approx \bar{\mathbf{N}}(\mathbf{x})\delta\hat{\mathbf{u}}(t) \tag{4.6}$$

$$\delta\mathbf{v}(\mathbf{x},t) \approx \bar{\mathbf{N}}(\mathbf{x})\delta\hat{\mathbf{v}}(t) \tag{4.7}$$

$$\delta\mathbf{a}(\mathbf{x},t) \approx \bar{\mathbf{N}}(\mathbf{x})\delta\hat{\mathbf{a}}(t) \tag{4.8}$$

The interpolation function or the shape function matrix $\bar{\mathbf{N}}$ has the following form

$$\bar{\mathbf{N}}(\mathbf{x}) = \left[\bar{\mathbf{N}}_1(\mathbf{x})\ \bar{\mathbf{N}}_2(\mathbf{x})\ \ ...\ \ ...\ \ \bar{\mathbf{N}}_{nT}(\mathbf{x})\right] \tag{4.9}$$

with

$$\bar{\mathbf{N}}_i(\mathbf{x}) = \begin{bmatrix}\bar{N}_i(x) & 0 & 0\\ 0 & \bar{N}_i(x) & 0\\ 0 & 0 & \bar{N}_i(x)\end{bmatrix} \tag{4.10}$$

with nT denoting the total number of nodes in the mesh. The bar superscript implies that the shape functions are written in terms of the global coordinate system. The vectors of nodal displacements, velocities and accelerations are denoted as $\hat{\mathbf{u}}$, $\hat{\mathbf{v}}$ and $\hat{\mathbf{a}}$, respectively. These vectors can be written as follows

$$\hat{\mathbf{u}}(t) = [\hat{u}_{11}\ \ \hat{u}_{12}\ \ \hat{u}_{13}\ \ ...\ \ ...\ \ ...\ \ \hat{u}_{n_T1}\ \ \hat{u}_{n_T2}\ \ \hat{u}_{n_T3}]^T \tag{4.11}$$

$$\hat{\mathbf{v}}(t) = [\hat{v}_{11}\ \ \hat{v}_{12}\ \ \hat{v}_{13}\ \ ...\ \ ...\ \ ...\ \ \hat{v}_{n_T1}\ \ \hat{v}_{n_T2}\ \ \hat{v}_{n_T3}]^T \tag{4.12}$$

$$\hat{\mathbf{a}}(t) = [\hat{a}_{11}\ \ \hat{a}_{12}\ \ \hat{a}_{13}\ \ ...\ \ ...\ \ ...\ \ \hat{a}_{n_T1}\ \ \hat{a}_{n_T2}\ \ \hat{a}_{n_T3}]^T \tag{4.13}$$

where$v_{12}$ indicating the velocity at node 1 in the direction of coordinate $x_2$.

The kinematic relation can be written using matrix notation as

$$\dot{\boldsymbol{\varepsilon}}(\mathbf{x},t) = \mathbf{L}\mathbf{v}(\mathbf{x},t) \tag{4.14}$$

with $\mathbf{L}$ being a linear differential operator, that has the following form

$$\mathbf{L} = \begin{bmatrix}\frac{\partial}{\partial x_1} & 0 & 0\\ 0 & \frac{\partial}{\partial x_2} & 0\\ 0 & 0 & \frac{\partial}{\partial x_3}\\ \frac{\partial}{\partial x_2} & \frac{\partial}{\partial x_1} & 0\\ 0 & \frac{\partial}{\partial x_3} & \frac{\partial}{\partial x_2}\\ \frac{\partial}{\partial x_3} & 0 & \frac{\partial}{\partial x_1}\end{bmatrix} \tag{4.15}$$

Substituting the second of Equation (4.3.1) into Equation (4.14) yields

$$\dot{\boldsymbol{\varepsilon}}(\mathbf{x},t) = \mathbf{L}\mathbf{N}(\mathbf{x})\hat{\mathbf{v}}(t) = \mathbf{B}(\mathbf{x})\hat{\mathbf{v}}(t) \tag{4.16}$$

in which $\mathbf{B}$ is the strain-displacement matrix that can be written as

$$\mathbf{B}(\mathbf{x}) = [\mathbf{B}_1(\mathbf{x}) \;\; \mathbf{B}_2(\mathbf{x}) \;\; \mathbf{B}_3(\mathbf{x}) \;\; ... \;\; ... \;\; ... \;\; \mathbf{B}_{nT}(\mathbf{x})] \tag{4.17}$$

with

$$\mathbf{B}_i(\mathbf{x}) = \begin{bmatrix} \frac{\partial \bar{N}_i(\mathbf{x})}{\partial x_1} & 0 & 0 \\ 0 & \frac{\partial \bar{N}_i(\mathbf{x})}{\partial x_2} & 0 \\ 0 & 0 & \frac{\partial \bar{N}_i(\mathbf{x})}{\partial x_3} \\ \frac{\partial \bar{N}_i(\mathbf{x})}{\partial x_2} & \frac{\partial \bar{N}_i(\mathbf{x})}{\partial x_1} & 0 \\ 0 & \frac{\partial \bar{N}_i(\mathbf{x})}{\partial x_3} & \frac{\partial \bar{N}_i(\mathbf{x})}{\partial x_2} \\ \frac{\partial \bar{N}_i(\mathbf{x})}{\partial x_3} & 0 & \frac{\partial \bar{N}_i(\mathbf{x})}{\partial x_1} \end{bmatrix} \tag{4.18}$$

The weak form yields as follow:

$$\begin{aligned} &\delta\hat{\mathbf{v}}^T \int_{\partial\Omega} \bar{\mathbf{N}}^T \mathbf{t} \cdot \mathbf{n} \, d\partial\Omega - \delta\hat{\mathbf{v}}^T \int_{\Omega} B^T \boldsymbol{\sigma} \, d\Omega + \\ &+\delta\hat{\mathbf{v}}^T \int_{\Omega} \bar{\mathbf{N}}^T \rho \mathbf{g} \, d\Omega - \delta\hat{\mathbf{v}}^T \left[ \int_{\Omega} \bar{\mathbf{N}}^T \rho \bar{\mathbf{N}} \, d\Omega \right] \hat{\mathbf{a}} = \mathbf{0} \end{aligned} \tag{4.19}$$

where $\mathbf{n}$ is the unit vector which is normal to the boundary of the domain.

The discretized form yields:

$$\mathbf{f}^{ext} - \mathbf{f}^{int} = \mathbf{M}\hat{\mathbf{a}} \tag{4.20}$$

with

$$\mathbf{f}^{ext} = \int_{\partial\Omega} \bar{\mathbf{N}}^T \mathbf{t} \cdot \mathbf{n} \, d\partial\Omega + \int_{\Omega} \rho \bar{\mathbf{N}}^T \mathbf{g} \, d\Omega \tag{4.21}$$

$$\mathbf{f}^{int} = \int_{\Omega} \mathbf{B}^T \boldsymbol{\sigma}' \, d\Omega \tag{4.22}$$

$$\mathbf{M} = \int_{\Omega} \rho \bar{\mathbf{N}}^T \bar{\mathbf{N}} d\Omega \tag{4.23}$$

where $\mathbf{f}^{ext}$ is the vector of nodal external forces, $\mathbf{f}^{int}$ is the vector of nodal internal forces and $\mathbf{M}$ is the nodal mass matrix.

### 4.3.2 Initialization of material points

The MP carry all the information of the continuum. In this section, we discuss the initialization of MP within the background mesh. This includes association of mass, body forces, tractions and other properties of the continuum to MP. Elements filled with MP are called active elements and their nodes contribute to the solving system of equations; on the contrary the empty elements, i.e. those without any MP, are ignored thus reducing the computational cost.

Let us consider a single tetrahedral element to explain the full procedure of initialization of MP information. Each MP is initially positioned at a predefined local position inside the parent

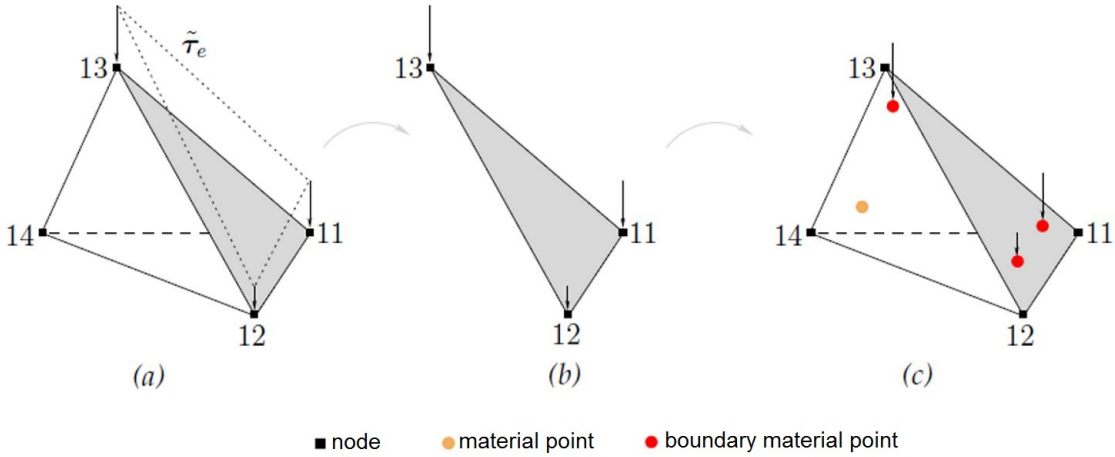


***Figure 4.1:*** *Initialization of surface traction. (a) tetrahedral element (b) triangular element (c) traction is mapped to the boundary MP, after [10].*

element, and hence the local position vector $\boldsymbol{\xi}_{MP}$ of the material point MP is initialized. The global position vector $\mathbf{x}_{MP}$ is then obtained as

$$\mathbf{x}_{MP}(\boldsymbol{\xi}_{MP}) \approx \sum_{i=1}^{no_{nodes}} N_i(\boldsymbol{\xi}_{MP}^t)\mathbf{x}_i \tag{4.24}$$

in which $no_{nodes}$ denotes the number of nodes per element, $N_i(\boldsymbol{\xi}_{MP})$ is the shape function of node i evaluated at the local position of material point MP and $\mathbf{x}_i$ are the nodal coordinates.

Volumes associated with MP are calculated so that all the MP inside the element have initially the same portion of the element volume, i.e.

$$\Omega_{MP} = \frac{1}{no_{MP,el}} \int_{\Omega_e} d\Omega \approx \frac{1}{no_{MP,el}} \sum_{q=1}^{n_{q,el}} w_{MP} \, |\mathbf{J}(\boldsymbol{\xi}_{MP})| \tag{4.25}$$

where $\Omega_{MP}$ is the volume associated with the material point MP, $no_{MP,el}$ denotes the number of MP in the element, $no_{q,el}$ is the number of Gauss points in the element, $w_{MP}$ is the local integration weight associated with Gauss point MP, and $\mathbf{J}$ is the Jacobian matrix. This implies that, at the beginning of the calculation, all the active elements are assumed to be fully filled by the continuum body. An element is said to be partially filled if the sum of the volumes of the contained MP is less than the element volume.

The mass $m_{MP}$ is then calculated as

$$m_{MP} = \Omega_{MP} \rho_{MP} \tag{4.26}$$

with $\rho$ being the mass density of the material to which the material point MP belongs.

The gravity force $\mathbf{f}_{MP}^{grav}$ is simply calculated using the mass of the MP and the vector of gravitational acceleration $\mathbf{g}$ as

$$\mathbf{f}_{MP}^{grav} = m_{MP}\mathbf{g} \tag{4.27}$$

The external forces applied at the traction boundary are mapped to the MP located next to the element border, also called boundary MP (Fig. 4.1).

These MP carry surface traction throughout the computations. Considering a tetrahedral element, the traction vector $\tau_e$ applied at the triangular surface is interpolated from the nodes of this surface to the boundary MP. Hence, the traction at boundary material point MP is

$$\tau_e(\mathbf{x}_p) \approx \sum_{i=1}^{n_{tri}} N_i(\xi_q)\tau_e(\mathbf{x}_i) \tag{4.28}$$

where $N_i$ is the shape function of node i of the triangular surface element and $\xi_q$ are the coordinates of the boundary MP p inside the parent triangular element. These coordinates simply represent the projection of the MP on the triangular surface element. The traction force vector $\mathbf{f}_p^{trac}$ is then

$$\mathbf{f}_p^{trac} = \tau_e(\mathbf{x}_{MP})\frac{S_e}{n_{ebMP}} = \frac{S_e}{n_{ebMP}}\sum_{i=1}^{n_{tri}} N_i(\xi_{MP})\tau_e(\mathbf{x}_i) \tag{4.29}$$

in which $n_{ebMP}$ denotes the number of boundary MP located next to the loaded surface and $S_e$ is the area of the corresponding loaded surface of the element e.

In the initialization of MP, initial conditions, material parameters and constitutive variables are assigned to them as well. Furthermore, book-keeping is initialized at this step, including information such as to which element each particle initially belongs and the initial number of particles per each active finite element.

### 4.3.3 Calculation of internal forces

In finite element formulation the numerical integration of all integrals above is not performed along the global coordinate system. Usually, it is more convenient to convert the global coordinates ($\mathbf{x}$) of each element into a reference (or *parent*) element system ($\xi$), and the mapping procedure is done using the *Jacobian matrix*. In this work, a unit 4-node tetrahedron with linear shape functions is chosen to be the reference element. Details about the mapping procedure are described in Section 4.7. The internal force becomes

$$\mathbf{f}^{int} = \sum_{el=1}^{no_{elm}} \int_{\Omega_{el}} \mathbf{B}^T\boldsymbol{\sigma}\, d\Omega = \sum_{el=1}^{no_{elm}} \int_{\square} \mathbf{B}^T\boldsymbol{\sigma}|J|\, d\square \tag{4.30}$$

where $\Omega_{el}$ is the volume of the element el in the global coordinate system, $no_{elm}$ is the number of active elements, $\square$ is volume of the parent element, $d\square = d\xi_1 d\xi_2 d\xi_3$ is the infinitesimal volume in the parent element system, $|J|$ is the determinant of the Jacobian, and $\mathbf{B}$ is the matrix of the shape function gradients calculated at location $\xi$ with respect to the parent coordinate system. If numerical integration is applied, the equations yield as follows

$$\mathbf{f}^{int} = \sum_{el=1}^{no_{elm}} \sum_{i=1}^{no_{Nodes,el}} \sum_{k=1}^{no_{int,el}} \mathbf{B}_i^T(\xi_k)\boldsymbol{\sigma}_k|J_k|W_k \tag{4.31}$$

where $no_{Nodes,el}$ and $no_{int,el}$ are respectively the number of nodes and integration points inside the element el, and $W_k$ is the weight factor (or integration weight) of the integration point k.

In the material point method the MP carry all the information of the continuum, including the stresses. The internal forces are computed in the following form

$$\mathbf{f}^{\text{int}} = \sum_{\text{el}=1}^{\text{no}_{\text{elm}}} \sum_{\text{i}=1}^{\text{no}_{\text{Nodes,el}}} \sum_{\text{MP}=1}^{\text{no}_{\text{MP,el}}} \mathbf{B}_{\text{i}}^{\text{T}}(\boldsymbol{\xi}_{MP})\boldsymbol{\sigma}_{\text{MP}}\Omega_{\text{MP}} \tag{4.32}$$

where $\text{no}_{\text{MP,el}}$ is the number of material points within element el.

### 4.3.4 Calculation of external forces

The external forces can be subdivided in two parts. The body force, due to the gravity acceleration, and the external loading due to distributed forces applied to the body.

The body force can be computed in the following way

$$\mathbf{f}^{\text{ext,grav}} = \sum_{\text{el}=1}^{\text{no}_{\text{elm}}} \int_{\Omega_{\text{el}}} \rho\bar{\mathbf{N}}^{\text{T}}\mathbf{g}\, \text{d}\Omega = \sum_{\text{el}=1}^{\text{no}_{\text{elm}}} \int_{\square} \rho\mathbf{N}^{\text{T}}\mathbf{g}|\text{J}|\, \text{d}\square \tag{4.33}$$

where $\Omega_{\text{el}}$ is the volume of the element el in the global coordinate system, $\text{no}_{\text{elm}}$ is the number of active elements, $\square$ is volume of the parent element, $\text{d}\square = \text{d}\xi_1\text{d}\xi_2\text{d}\xi_3$ is the infinitesimal volume in the parent element system, $|\text{J}|$ is the determinant of the Jacobian, and $\mathbf{N}$ is the shape function matrix calculated at location $\boldsymbol{\xi}$ with respect to the parent coordinate system. Applying the material point integration, the equation yield as follows

$$\mathbf{f}^{\text{ext,grav}} = \sum_{\text{el}=1}^{\text{no}_{\text{elm}}} \sum_{\text{i}=1}^{\text{no}_{\text{Nodes,el}}} \sum_{\text{MP}=1}^{\text{no}_{\text{MP,el}}} \text{m}_{\text{MP}}\mathbf{N}_{\text{i}}^{\text{T}}(\boldsymbol{\xi}_{MP})\mathbf{g}\Omega_{\text{MP}} \tag{4.34}$$

where $\text{no}_{\text{Nodes,el}}$ and $\text{no}_{\text{MP,el}}$ are respectively the number of nodes and material points inside the element el.

The external forces due to traction are computed in the following way

$$\mathbf{f}^{\text{ext,trac}} = \sum_{\text{el}=1}^{\text{no}_{\text{elm}}} \int_{\partial\Omega_{\text{el}}} \bar{\mathbf{N}}^{\text{T}}\mathbf{t}\cdot\mathbf{n}\, \text{d}\partial\Omega = \sum_{\text{el}=1}^{\text{no}_{\text{elm}}} \sum_{\text{i}=1}^{\text{no}_{\text{Nodes,el}}} \sum_{\text{MP}=1}^{\text{no}_{\text{MP,el}}} \mathbf{N}^{\text{T}}(\boldsymbol{\xi}_{MP})\, \mathbf{f}_{\text{MP}}^{\text{ext}} \tag{4.35}$$

where $\mathbf{f}_{\text{MP}}^{\text{ext}}$ is the force stored in the material point due to distributed external forces applied at the boundary of the body, as described in Section 4.3.2.

The complete form of the external force is summarized below:

$$\mathbf{f}^{\text{ext}} = \sum_{\text{el}=1}^{\text{no}_{\text{elm}}} \sum_{\text{i}=1}^{\text{no}_{\text{Nodes,el}}} \sum_{\text{MP}=1}^{\text{no}_{\text{MP,el}}} \mathbf{N}^{\text{T}}(\boldsymbol{\xi}_{MP})\, \mathbf{f}_{\text{MP}}^{\text{ext,trac}} + \sum_{\text{el}=1}^{\text{no}_{\text{elm}}} \sum_{\text{i}=1}^{\text{no}_{\text{Nodes,el}}} \sum_{\text{MP}=1}^{\text{no}_{\text{MP,el}}} \text{m}_{\text{MP}}\mathbf{N}_{\text{i}}^{\text{T}}(\boldsymbol{\xi}_{MP})\mathbf{g}\Omega_{\text{MP}} \tag{4.36}$$

### 4.3.5 Mass matrix

To solve the system of equations (Eq. 4.20), the mass matrix has to be inverted. In practice, to simplify computations, a lumped mass matrix may be used instead of the consistent mass matrix given by Eq. 4.23. The lumped mass matrix is a diagonal matrix in which each entry $\text{m}_{\text{i}}$

is obtained by summing over the corresponding row of the consistent mass matrix. Matrix inversions become trivial, although the result of using a lumped mass matrix is some dissipation of kinetic energy that has been quantified by [11]. Using the property $\sum_{j=1}^{N_n} N_j^p = 1$ it becomes

$$\mathbf{M}^{\text{lump}} = \sum_{el=1}^{no_{elm}} \sum_{i=1}^{no_{Nodes,el}} \sum_{MP=1}^{no_{MP,el}} \mathbf{N}^T(\xi_{MP})\, m_{MP} \tag{4.37}$$

Hereinafter, the superscript lump is removed from the lumped mass matrix $\mathbf{M}^{\text{lump}}$ to simplify the notation, and mass matrix will always refer to a lumped matrix.

In this study the 4-node tetrahedral element is used and the lumping procedure gives the following expression for the mass matrix **M**.

$$\mathbf{M} = \sum_{el=1}^{n_{elm}} \mathbf{M}_{el} \tag{4.38}$$

$$\mathbf{M}_{el} = \begin{bmatrix} \mathbf{m}_1 & \mathbf{0} & \mathbf{0} & ... & \mathbf{0} \\ \mathbf{0} & \mathbf{m}_2 & \mathbf{0} & ... & \mathbf{0} \\ \mathbf{0} & ... & ... & \mathbf{m}_i & \mathbf{0} \\ \mathbf{0} & \mathbf{0} & \mathbf{0} & ... & \mathbf{m}_{\text{NodeEl}} \end{bmatrix} \tag{4.39}$$

$$\mathbf{m}_i = \begin{bmatrix} m_i & 0 & 0 \\ 0 & m_i & 0 \\ 0 & 0 & m_i \end{bmatrix} ; \mathbf{0} = \begin{bmatrix} 0 & 0 & 0 \\ 0 & 0 & 0 \\ 0 & 0 & 0 \end{bmatrix} \tag{4.40}$$

$$m_i = \sum_{MP=1}^{no_{MP,el}} m_{MP} N_i(\xi_{MP}) \tag{4.41}$$

### 4.3.6 Time discretization

The time has been discretized into different instants (k). Considering $\Delta t$ the time step size, the time discretization approach is $t^{k+1} = t^k + \Delta t$.

If the general system of equations (Eq. 4.20) is posed at time $t^k$, it can be rewritten as shown in Eq. 4.42, where the acceleration $\hat{\mathbf{a}}^k$ is the unknown.

$$\mathbf{M}^k \cdot \hat{\mathbf{a}}^k = \mathbf{f}^{\text{int}^k} + \mathbf{f}^{\text{ext}^k} \tag{4.42}$$

An explicit Euler time integration scheme is used to update the velocity (Eq. 4.43). This is a first-order numerical procedure for solving ordinary differential equations (ODEs) with a given initial value. Being $\hat{\mathbf{v}}^k$ the velocity at time $t^k$, the velocity at the next time step $t^{k+1}$ is calculated using the acceleration at time $t^k$ as follows.

$$\hat{\mathbf{v}}^{k+1} = \hat{\mathbf{v}}^k + \triangle t\, \hat{\mathbf{a}}^k \tag{4.43}$$

On the other hand, the displacements at time $t^{k+1}$ are calculated using the updated velocity $\hat{\mathbf{v}}^{k+1}$ as indicated in Eq. 4.44.

$$\hat{\mathbf{u}}^{k+1} = \hat{\mathbf{u}}^k + \triangle t\, \hat{\mathbf{v}}^{k+1} \tag{4.44}$$

### 4.3.7 Solution algorithm for single timestep

The algorithm presented here is based on the work presented by [3], which was improved respected the original one [2]. The key point is to work with momentum instead of velocity as much as possible, thus avoiding divisions by nodal masses. In each time step, the MPM computational cycle can be listed as follows.

1 The nodal mass is calculated using the shape functions and the lumped mass matrix at time $t^k$ is formed (Eq. 4.37). The internal and external forces are evaluated in the nodes (Eqs.4.36 and 4.32).

2 The momentum balance equation (Eq. 4.42) is solved and the nodal accelerations $\hat{\mathbf{a}}_i^k$ are determined.

$$\hat{\mathbf{a}}_i^k = [\mathbf{M}_i^k]^{-1} \, (\mathbf{f}_i^{ext,k} - \mathbf{f}_i^{int,k}) \tag{4.45}$$

3 The velocity at the material points is updated considering Eq. 4.43 as

$$\mathbf{v}_{MP}^{k+1} = \mathbf{v}_{MP}^k + \Delta t \sum_{i=1}^{no_{Nodes}} N_i(\boldsymbol{\xi}_{MP}^k) \, \hat{\mathbf{a}}_i^k \tag{4.46}$$

4 Update nodal momentum

$$\mathbf{P}_i^{k+1} = \sum_{el=1}^{no_{el,i}} \sum_{MP=1}^{no_{MP,el}} m_{MP} \, N_j(\boldsymbol{\xi}_{MP}^k) \, \mathbf{v}_{MP}^{k+1} \tag{4.47}$$

5 Update nodal velocities

$$\hat{\mathbf{v}}_i^{k+1} = \frac{\mathbf{P}_i^{k+1}}{\mathbf{M}_i^k} \tag{4.48}$$

6 Compute incremental nodal displacement for solid and liquid constituent

$$\Delta\hat{\mathbf{u}}_i^{k+1} = \Delta t \, \hat{\mathbf{v}}_i^{k+1} \tag{4.49}$$

7 Compute strain increment

$$\Delta\varepsilon_{MP}^{k+1} = \mathbf{B}(\mathbf{x}_{MP})\Delta\hat{\mathbf{u}}_i{}^{k+1}$$

8 The stresses are updated using a material constitutive model

9 Update volume and density of MP

$$\Omega_{MP}^{k+1} = \Omega_{MP}^k(1 + \Delta\varepsilon_{vol,MP}) \qquad \rho_{MP}^{k+1} = \frac{\rho_{MP}^k}{(1 + \Delta\varepsilon_{vol,MP})} \tag{4.50}$$

10 Particle positions are updated considering Eq. 4.44 as

$$\mathbf{x}_{MP}^{k+1} = \mathbf{x}_{MP}^k + \sum_{i=1}^{no_{Nodes}} N_i(\boldsymbol{\xi}_{MP}^k) \, \Delta\hat{\mathbf{u}}_i^k \tag{4.51}$$

11 The computational grid is initialized for the next step, nodal values are discarded and the material points carry all the updated information.

### 4.3.8 Considerations on the use of 1-phase solid analysis with porous media

Porous media are, in general, a mixture of three phases (solid, liquid and gas), which interact between each other, thus determining the mechanical response of the system. Taking rigorously into account these interactions may be in many cases unacceptably complicated, computationally expensive, and even unnecessary for engineering applications. For example, in numerical analyses dealing with drained and undrained conditions the presence of the pore liquid (e.g. water) can be considered in a simplified way. In the first case, the excess pore pressure is assumed to be zero, thus the presence of the liquid can be neglected and the solid skeleton (e.g. soil) can be regarded as 1-phase even though it is saturated. In the latter, because of the negligible relative movement between solid and pore liquid, the equilibrium of the solid-liquid mixture can be considered rather than the equilibrium of solid skeleton and pore liquid as separate phases.

In undrained conditions, the stress state can be described in terms of total stresses or effective stresses. In the second case the excess pore pressures can be computed by means of the so-called Effective Stress Analysis, which is based on the assumption of strain compatibility between the solid skeleton and the enclosed liquid [12]. With the Effective Stress Analyses the pore pressure increment is computed as:

$$\Delta p = K_L \Delta \varepsilon_{vol} \tag{4.52}$$

where $\Delta \varepsilon_{vol}$ is the volumetric strain and $K_L$ is the bulk modulus of the liquid.

Modeling of dry soil, and saturated soil in drained and undrained conditions are the field of applicability of the 1-phase formulation. For partially drained conditions a fully-coupled 2-phase formulation is necessary. This is presented in Section 4.5.

## 4.4 Liquid analysis with material point method

### 4.4.1 Discretized momentum balance equation of liquid

The weak form can be written as follow:

$$\delta\hat{\mathbf{v}}_L^T \int_{\partial\Omega} \overline{\mathbf{N}}^T \mathbf{t}\cdot\mathbf{n}\, d\partial\Omega - \delta\hat{\mathbf{v}}_L^T \int_\Omega B^T \boldsymbol{\sigma}_L\, d\Omega + \\ +\delta\hat{\mathbf{v}}_L^T \int_\Omega \overline{\mathbf{N}}^T \rho_L \mathbf{g}\, d\Omega - \delta\hat{\mathbf{v}}_L^T \left[\int_\Omega \overline{\mathbf{N}}^T \rho_L \overline{\mathbf{N}}\, d\Omega\right] \dot{\hat{\mathbf{v}}}_L = \mathbf{0} \tag{4.53}$$

This equation has the same form as Eq. 4.3.1. More info about the derivation of the weak form of the momentum balance equation, the reader should refer to Sec.4.3.1.

The discretized form can be written in the following yields:

$$\mathbf{f}_L^{ext} - \mathbf{f}_L^{int} = \mathbf{M}_L \hat{\mathbf{a}} \tag{4.54}$$

with

$$\mathbf{f}_L^{ext} = \int_{\partial\Omega} \overline{\mathbf{N}}^T \mathbf{t}_L \cdot \mathbf{n}\, d\partial\Omega + \int_\Omega \rho_L \overline{\mathbf{N}}^T \mathbf{g}\, d\Omega \tag{4.55}$$

$$\mathbf{f}_L^{int} = \int_\Omega \mathbf{B}^T \boldsymbol{\sigma}_L\, d\Omega \tag{4.56}$$

$$\mathbf{M}_L = \int_\Omega \rho_L \overline{\mathbf{N}}^T \overline{\mathbf{N}} d\Omega \tag{4.57}$$

where $\mathbf{f}_L^{ext}$ is the vector of nodal external forces, $\mathbf{f}_L^{int}$ is the vector of nodal internal forces and $\mathbf{M}_L$ is the nodal mass matrix.

### 4.4.2 Calculation of internal forces

In finite element formulation the numerical integration of all integrals above is usually performed using a reference (or *parent*) element system ($\boldsymbol{\xi}$), and the mapping procedure is done using the *Jacobian matrix*. In this manual, a unit 4-node tetrahedron with linear shape functions is chosen to be the reference element. Details about the calculation of the internal forces are discussed in Section 4.3.3 and details about the mapping procedure are described in Section 4.7.

The internal force vector becomes

$$\mathbf{f}_L^{int} = \sum_{el=1}^{no_{elm}} \int_{\Omega_{el}} \mathbf{B}^T \boldsymbol{\sigma}_L\, d\Omega = \sum_{el=1}^{no_{elm}} \int_\square \mathbf{B}^T \boldsymbol{\sigma}_L |J|\, d\square \tag{4.58}$$

where $\Omega_{el}$ is the volume of the element el in the global coordinate system, $no_{elm}$ is the number of active elements, $\square$ is volume of the parent element, $d\square = d\xi_1 d\xi_2 d\xi_3$ is the infinitesimal volume in the parent element system, $|J|$ is the determinant of the Jacobian, and $\mathbf{B}$ is the matrix of shape function gradients calculated at location $\boldsymbol{\xi}$ with respect to the parent coordinate system.

In the material point method the MP carry all the information of the continuum, including the stresses. Thus, the internal forces are computed in the following form

$$\mathbf{f}_{\mathrm{L}}^{\mathrm{int}} = \sum_{\mathrm{el}=1}^{\mathrm{no_{elm}}} \sum_{\mathrm{i}=1}^{\mathrm{no_{Nodes,el}}} \sum_{\mathrm{MP}=1}^{\mathrm{no_{MP,el}}} \mathbf{B}_{\mathrm{i}}^{\mathrm{T}}(\boldsymbol{\xi}_{MP})\boldsymbol{\sigma}_{\mathrm{L,MP}}\Omega_{\mathrm{MP}} \tag{4.59}$$

where $\mathrm{no_{MP,el}}$ is the number of material points within element el.

### 4.4.3 Calculation of external forces

As for the 1-phase-solid formulation, the external forces can be subdivided in two parts: the body force, which is generated by gravity acceleration, and the external loading due to distributed forces applied to the boundary of the liquid body.

The body force can be computed in the following way

$$\mathbf{f}_{\mathrm{L}}^{\mathrm{ext,grav}} = \sum_{\mathrm{el}=1}^{\mathrm{no_{elm}}} \int_{\Omega_{\mathrm{el}}} \rho_{\mathrm{L}} \bar{\mathbf{N}}^{\mathrm{T}} \mathbf{g} \, \mathrm{d}\Omega = \sum_{\mathrm{el}=1}^{\mathrm{no_{elm}}} \int_{\square} \rho \mathbf{N}^{\mathrm{T}} \mathbf{g} |\mathrm{J}| \, \mathrm{d}\square \tag{4.60}$$

where $\Omega_{\mathrm{el}}$ is the volume of the element el in the global coordinate system, $\mathrm{no_{elm}}$ is the number of active elements, $\square$ is volume of the parent element, $\mathrm{d}\square = \mathrm{d}\xi_1\mathrm{d}\xi_2\mathrm{d}\xi_3$ is the infinitesimal volume in the parent element system, $|\mathrm{J}|$ is the determinant of the Jacobian, and $\mathbf{N}$ is the shape function matrix calculated at location $\boldsymbol{\xi}$ with respect to the parent coordinate system. Applying the material point integration, the equation yield as follows

$$\mathbf{f}_{\mathrm{L}}^{\mathrm{ext,grav}} = \sum_{\mathrm{el}=1}^{\mathrm{no_{elm}}} \sum_{\mathrm{i}=1}^{\mathrm{no_{Nodes,el}}} \sum_{\mathrm{MP}=1}^{\mathrm{no_{MP,el}}} \mathrm{m_{MP}} \mathbf{N}_{\mathrm{i}}^{\mathrm{T}}(\boldsymbol{\xi}_{MP}) \mathbf{g} \Omega_{\mathrm{MP}} \tag{4.61}$$

where $\mathrm{no_{Nodes,el}}$ and $\mathrm{no_{MP,el}}$ are respectively the number of nodes and material points inside the element el.

The external forces due to traction are computed in the following way

$$\mathbf{f}_{\mathrm{L}}^{\mathrm{ext,trac}} = \sum_{\mathrm{el}=1}^{\mathrm{no_{elm}}} \int_{\partial\Omega_{\mathrm{el}}} \bar{\mathbf{N}}^{\mathrm{T}} \mathbf{t}_{\mathrm{L}} \cdot \mathbf{n} \, \mathrm{d}\partial\Omega = \sum_{\mathrm{el}=1}^{\mathrm{no_{elm}}} \sum_{\mathrm{i}=1}^{\mathrm{no_{Nodes,el}}} \sum_{\mathrm{MP}=1}^{\mathrm{no_{MP,el}}} \mathbf{N}^{\mathrm{T}}(\boldsymbol{\xi}_{MP}) \, \mathbf{f}_{\mathrm{L,MP}}^{\mathrm{ext,trac}} \tag{4.62}$$

where $\mathbf{f}_{\mathrm{L,MP}}^{\mathrm{ext}}$ is the force stored in the material point due to distributed external forces applied at the boundary of the body, as described in Section 4.3.2.

The complete form of the external force is summarized below:

$$\mathbf{f}_{\mathrm{L}}^{\mathrm{ext}} = \sum_{\mathrm{el}=1}^{\mathrm{no_{elm}}} \sum_{\mathrm{i}=1}^{\mathrm{no_{Nodes,el}}} \sum_{\mathrm{MP}=1}^{\mathrm{no_{MP,el}}} \mathbf{N}^{\mathrm{T}}(\boldsymbol{\xi}_{MP}) \, \mathbf{f}_{\mathrm{MP}}^{\mathrm{ext}} + \sum_{\mathrm{el}=1}^{\mathrm{no_{elm}}} \sum_{\mathrm{i}=1}^{\mathrm{no_{Nodes,el}}} \sum_{\mathrm{MP}=1}^{\mathrm{no_{MP,el}}} \mathrm{m_{MP}} \mathbf{N}_{\mathrm{i}}^{\mathrm{T}}(\boldsymbol{\xi}_{MP}) \mathbf{g} \Omega_{\mathrm{MP}} \tag{4.63}$$

### 4.4.4 Mass matrix

To solve the system of equations (Eq. 4.54), the mass matrix has to be inverted. In practice, to simplify computations, a lumped mass matrix may be used instead of the consistent mass matrix given by Eq. 4.57. The lumped mass matrix is a diagonal matrix in which each entry $m_i$ is obtained by summing over the corresponding row of the consistent mass matrix. Matrix inversions become trivial, although the result of using a lumped mass matrix is some dissipation of kinetic energy that has been quantified by [11]. Using the property $\sum_{MP=1}^{no_{MP}} N_i(\xi_{MP}) = 1$ it becomes

$$\mathbf{M}_L^{lump} = \sum_{el=1}^{no_{elm}} \sum_{i=1}^{no_{Nodes,el}} \sum_{MP=1}^{no_{MP,el}} \mathbf{N}^T(\xi_{MP})\, m_{MP} \tag{4.64}$$

Hereinafter, the superscript lump is removed from the lumped mass matrix $\mathbf{M}^{lump}$ to simplify the notation, and mass matrix always will refer to a lumped matrix.

In this study the 4-node tetrahedral element is used and the lumping procedure gives the following expression for the mass matrix **M**.

$$\mathbf{M}_L = \sum_{el=1}^{n_{elm}} \mathbf{M}_{L,el} \tag{4.65}$$

$$\mathbf{M}_{L,el} = \begin{bmatrix} \mathbf{m}_1 & \mathbf{0} & \mathbf{0} & \dots & \mathbf{0} \\ \mathbf{0} & \mathbf{m}_2 & \mathbf{0} & \dots & \mathbf{0} \\ \mathbf{0} & \dots & \dots & \mathbf{m}_i & \mathbf{0} \\ \mathbf{0} & \mathbf{0} & \mathbf{0} & \dots & \mathbf{m}_{NodeEl} \end{bmatrix} \tag{4.66}$$

$$\mathbf{m}_i = \begin{bmatrix} m_i & 0 & 0 \\ 0 & m_i & 0 \\ 0 & 0 & m_i \end{bmatrix} \; ; \; \mathbf{0} = \begin{bmatrix} 0 & 0 & 0 \\ 0 & 0 & 0 \\ 0 & 0 & 0 \end{bmatrix} \tag{4.67}$$

$$m_i = \sum_{MP=1}^{no_{MP,el}} m_{MP} N_i(\xi_{MP}) \tag{4.68}$$

#### 4.4.4.1 Time discretization

The time has been discretized into different instants (k). Considering $\Delta t$ the time step size, the time discretization approach is $t^{k+1} = t^k + \Delta t$.

If the general system of equations (Eq. 4.54) is posed at time $t^k$, it can be rewritten as Eq. 4.42, where the acceleration $\hat{\mathbf{a}}^k$ is the unknown.

$$\mathbf{M}_L^k \cdot \hat{\mathbf{a}}_L^k = \mathbf{f}_L^{int^k} + \mathbf{f}_L^{ext^k} \tag{4.69}$$

An explicit Euler time integration scheme is used to update the velocity (Eq. 4.43). This is a first-order numerical procedure for solving ordinary differential equations (ODEs) with a given initial value. Being $\hat{\mathbf{v}}^k$ the velocity at time $t^k$, the velocity at the next time step $t^{k+1}$ is calculated using the acceleration at time $t^k$ as follows.

$$\hat{\mathbf{v}}_L^{k+1} = \hat{\mathbf{v}}_L^k + \triangle t\, \hat{\mathbf{a}}_L^k \tag{4.70}$$

On the other hand, the displacements at time $t^{k+1}$ are calculated using the updated velocity $\hat{\mathbf{v}}_L^{k+1}$ as indicated in Eq. 4.71.

$$\hat{\mathbf{u}}_L^{k+1} = \hat{\mathbf{u}}_L^k + \triangle t\, \hat{\mathbf{v}}_L^{k+1} \tag{4.71}$$

### 4.4.5 Solution algorithm for single timestep

The algorithm presented here is based on the work presented by [3], which was improved respected the original one [2]. The key point is to work with momentum instead of velocity as much as possible, thus avoiding divisions by nodal masses. In each time step, the MPM computational cycle can be listed as follows.

1 The nodal mass is calculated using the shape functions and the lumped mass matrix at time $t^k$ is formed (Eq. 4.64). The internal and external forces are evaluated in the nodes (Eqs. 4.63 and 4.59).

2 The momentum balance equation (Eq. 4.69) is solved and the nodal accelerations $\hat{\mathbf{a}}^k_{L,i}$ are determined.

$$\hat{\mathbf{a}}^k_{L,i} = [\mathbf{M}^k_{L,i}]^{-1} \, (\mathbf{f}^{ext,k}_{L,i} - \mathbf{f}^{int,k}_{L,i}) \tag{4.72}$$

3 The velocity at the material points is updated considering Eq. 4.70 as

$$\mathbf{v}^{k+1}_{MP} = \mathbf{v}^k_{MP} + \Delta t \sum_{i=1}^{no_{Nodes}} N_i(\xi^k_{MP}) \, \hat{\mathbf{a}}^k_{L,i} \tag{4.73}$$

4 Update nodal momentum

$$\mathbf{P}^{k+1}_{L,i} = \sum_{el=1}^{no_{el,i}} \sum_{MP=1}^{no_{MP,el}} m_{MP} \, N_j(\xi^k_{MP}) \, \mathbf{v}^{k+1}_{MP} \tag{4.74}$$

5 Update nodal velocities

$$\hat{\mathbf{v}}^{k+1}_{L,i} = \frac{\mathbf{P}^{k+1}_{L,i}}{\mathbf{M}^k_{L,i}} \tag{4.75}$$

6 . Compute incremental nodal displacement

$$\Delta\hat{\mathbf{u}}^{k+1}_{L,i} = \Delta t \, \hat{\mathbf{v}}^{k+1}_{L,i} \tag{4.76}$$

7 . Compute strain increment

$$\Delta\varepsilon^{k+1}_{MP} = \mathbf{B}(\mathbf{x}_{MP})\Delta\hat{\mathbf{u}}^{k+1}_{L,i}$$

8 The stresses are updated using a material constitutive model of water described in Section 7.2.

9 Update volume and density of MP

$$\Omega^{k+1}_{MP} = \Omega^k_{MP}(1 + \Delta\varepsilon_{vol,MP}) \qquad \rho^{k+1}_{MP} = \frac{\rho^k_{MP}}{(1 + \Delta\varepsilon_{vol,MP})} \tag{4.77}$$

10 Particle positions are updated considering Eq. 4.44 as

$$\mathbf{x}^{k+1}_{MP} = \mathbf{x}^k_{MP} + \sum_{i=1}^{no_{Nodes}} N_i(\xi^k_{MP}) \, \Delta\hat{\mathbf{u}}^k_{L,i} \tag{4.78}$$

11 The computational grid is initialized for the next step, nodal values are discarded and the material points carry all the updated information.

## 4.5 2-phase-coupled with single material point

### 4.5.1 Discretized momentum balance equation of liquid phase

The weak form can be written as follow:

$$\delta\hat{\mathbf{v}}_L^T \int_{\partial\Omega} \overline{\mathbf{N}}^T \mathbf{t}_L \cdot \mathbf{n}\, d\partial\Omega - \delta\hat{\mathbf{v}}_L^T \int_\Omega B^T p_L \boldsymbol{\delta}\, d\Omega - \delta\hat{\mathbf{v}}_L^T \left[\int_\Omega \overline{\mathbf{N}}^T n \frac{\rho_L g}{k} \overline{\mathbf{N}}\, d\Omega\right] (\hat{\mathbf{v}}_L - \hat{\mathbf{v}}_S) +$$
$$+\delta\hat{\mathbf{v}}_L^T \int_\Omega \overline{\mathbf{N}}^T \rho_L \mathbf{g}\, d\Omega - \delta\hat{\mathbf{v}}_L^T \left[\int_\Omega \overline{\mathbf{N}}^T \rho_L \overline{\mathbf{N}}\, d\Omega\right] \hat{\mathbf{a}}_L = \mathbf{0} \tag{4.79}$$

in which $\boldsymbol{\delta} = \begin{bmatrix}1 & 1 & 1 & 0 & 0 & 0\end{bmatrix}^T$.

The discretized form can be written in the following yields:

$$\mathbf{f}_L^{ext} - \mathbf{f}_L^{int} - \mathbf{f}^d = \mathbf{M}_L \hat{\mathbf{a}} \tag{4.80}$$

with

$$\mathbf{f}_L^{ext} = \int_{\partial\Omega} \overline{\mathbf{N}}^T \mathbf{t}_L \cdot \mathbf{n}\, d\partial\Omega + \int_\Omega \rho_L \overline{\mathbf{N}}^T \mathbf{g}\, d\Omega \tag{4.81}$$

$$\mathbf{f}_L^{int} = \int_\Omega \mathbf{B}^T \boldsymbol{\sigma}_L\, d\Omega \tag{4.82}$$

$$\mathbf{f}^d = \int_\Omega \overline{\mathbf{N}}^T n \frac{\rho_L g}{k} \overline{\mathbf{N}}\, d\Omega\, (\hat{\mathbf{v}}_L - \hat{\mathbf{v}}_S) \tag{4.83}$$

$$\mathbf{M}_L = \int_\Omega \rho_L \overline{\mathbf{N}}^T \overline{\mathbf{N}} d\Omega \tag{4.84}$$

where $\mathbf{f}_L^{ext}$ is the vector of nodal external forces, $\mathbf{f}_L^{int}$ is the vector of nodal internal forces, $\mathbf{f}^d$ is the vector of drag forces and $\mathbf{M}_L$ is the nodal mass matrix.

### 4.5.2 Discretized momentum balance equation of mixture

The weak form can be written as follow:

$$\delta\hat{\mathbf{v}}_S^T \int_{\partial\Omega} \overline{\mathbf{N}}^T \mathbf{t} \cdot \mathbf{n}\, d\partial\Omega - \delta\hat{\mathbf{v}}_S^T \int_\Omega B^T \boldsymbol{\sigma}\, d\Omega +$$
$$+ \delta\hat{\mathbf{v}}_S^T \int_\Omega \overline{\mathbf{N}}^T \rho \mathbf{g}\, d\Omega - \delta\hat{\mathbf{v}}_S^T \left[\int_\Omega \overline{\mathbf{N}}^T n\, \rho_L \overline{\mathbf{N}}\, d\Omega\right] \hat{\mathbf{a}}_L - \delta\hat{\mathbf{v}}_S^T \left[\int_\Omega \overline{\mathbf{N}}^T (1-n)\, \rho_S \overline{\mathbf{N}}\, d\Omega\right] \hat{\mathbf{a}}_S = \mathbf{0} \tag{4.85}$$

The discretized form can be written in the following yields:

$$\mathbf{f}^{ext} - \mathbf{f}^{int} - \bar{\mathbf{M}}_L \hat{\mathbf{a}}_L = \mathbf{M}_S \hat{\mathbf{a}}_S \tag{4.86}$$

with

$$\mathbf{f}^{\text{ext}} = \int_{\partial\Omega} \bar{\mathbf{N}}^{\mathsf{T}} \mathbf{t} \cdot \mathbf{n} \, \mathrm{d}\partial\Omega + \int_{\Omega} \rho \bar{\mathbf{N}}^{\mathsf{T}} \mathbf{g} \, \mathrm{d}\Omega \tag{4.87}$$

$$\mathbf{f}^{\text{int}} = \int_{\Omega} \mathbf{B}^{\mathsf{T}} \boldsymbol{\sigma} \, \mathrm{d}\Omega \tag{4.88}$$

$$\bar{\mathbf{M}}_{\mathsf{L}} = \int_{\Omega} \bar{\mathbf{N}}^{\mathsf{T}} \mathrm{n} \, \rho_{\mathsf{L}} \bar{\mathbf{N}} \, \mathrm{d}\Omega \tag{4.89}$$

$$\mathbf{M}_{\mathsf{S}} = \int_{\Omega} (1 - \mathrm{n}) \rho_{\mathsf{S}} \bar{\mathbf{N}}^{\mathsf{T}} \bar{\mathbf{N}} \mathrm{d}\Omega \tag{4.90}$$

where $\mathbf{f}^{\text{ext}}$ is the vector of nodal external forces, $\mathbf{f}^{\text{int}}$ is the vector of nodal internal forces, $\bar{\mathbf{M}}_{\mathsf{L}}$ is the nodal mass matrix (including porosity) of the liquid phase and $\mathbf{M}_{\mathsf{S}}$ is the nodal mass matrix of the solid phase.

### 4.5.3 Calculation of internal forces

In finite element formulation the numerical integration of all integrals above is usually performed using a reference (or *parent*) element system ($\boldsymbol{\xi}$), and the mapping procedure is done using the *Jacobian matrix*. In this manual, a unit 4-node tetrahedron with linear shape functions is chosen to be the reference element. Details about the calculation of the internal forces are discussed in Section 4.3.3 and details about the mapping procedure are described in Section 4.7.

The internal force vector becomes

$$\mathbf{f}_{\mathsf{L}}^{\text{int}} = \sum_{\text{el}=1}^{\text{no}_{\text{elm}}} \int_{\Omega_{\text{el}}} \mathbf{B}^{\mathsf{T}} \boldsymbol{\sigma}_{\mathsf{L}} \, \mathrm{d}\Omega = \sum_{\text{el}=1}^{\text{no}_{\text{elm}}} \int_{\square} \mathbf{B}^{\mathsf{T}} \boldsymbol{\sigma}_{\mathsf{L}} |\mathrm{J}| \, \mathrm{d}\square \tag{4.91}$$

where $\Omega_{\text{el}}$ is the volume of the element el in the global coordinate system, $\text{no}_{\text{elm}}$ is the number of active elements, $\square$ is volume of the parent element, $\mathrm{d}\square = \mathrm{d}\xi_1 \mathrm{d}\xi_2 \mathrm{d}\xi_3$ is the infinitesimal volume in the parent element system, $|\mathrm{J}|$ is the determinant of the Jacobian, and $\mathbf{B}$ is the matrix of the shape function gradients calculated at location $\boldsymbol{\xi}$ with respect to the parent coordinate system.

In the material point method the MP carry all the information of the continuum, including the stresses. Thus, the internal forces are computed in the following form

$$\mathbf{f}_{\mathsf{L}}^{\text{int}} = \sum_{\text{el}=1}^{\text{no}_{\text{elm}}} \sum_{\mathrm{i}=1}^{\text{no}_{\text{Nodes,el}}} \sum_{\text{MP}=1}^{\text{no}_{\text{MP,el}}} \mathbf{B}_{\mathrm{i}}^{\mathsf{T}}(\boldsymbol{\xi}_{MP}) \boldsymbol{\sigma}_{\mathsf{L,MP}} \Omega_{\text{MP}} \tag{4.92}$$

where $\text{no}_{\text{MP,el}}$ is the number of material points within element el.

### 4.5.4 Calculation of external forces

As for the 1-phase-solid formulation, the external forces can be subdivided in two parts: the body force, which is generated by gravity acceleration, and the external loading due to distributed forces applied to the boundary of the liquid body.

The body force can be computed in the following way

$$\mathbf{f}_{L}^{ext,grav} = \sum_{el=1}^{no_{elm}} \int_{\Omega_{el}} \rho_{L} \bar{\mathbf{N}}^{T} \mathbf{g} \, d\Omega = \sum_{el=1}^{no_{elm}} \int_{\square} \rho \mathbf{N}^{T} \mathbf{g} |J| \, d\square \tag{4.93}$$

where $\Omega_{el}$ is the volume of the element el in the global coordinate system, $no_{elm}$ is the number of active elements, $\square$ is volume of the parent element, $d\square = d\xi_1 d\xi_2 d\xi_3$ is the infinitesimal volume in the parent element system, $|J|$ is the determinant of the Jacobian, and $\mathbf{N}$ is the shape function matrix calculated at location $\boldsymbol{\xi}$ with respect to the parent coordinate system. Applying the material point integration, the equation yield as follows

$$\mathbf{f}_{L}^{ext,grav} = \sum_{el=1}^{no_{elm}} \sum_{i=1}^{no_{Nodes,el}} \sum_{MP=1}^{no_{MP,el}} m_{MP} \mathbf{N}_{i}^{T}(\boldsymbol{\xi}_{MP}) \mathbf{g} \Omega_{MP} \tag{4.94}$$

where $no_{Nodes,el}$ and $no_{MP,el}$ are respectively the number of nodes and material points inside the element el.

The external forces due to traction are computed in the following way

$$\mathbf{f}_{L}^{ext,trac} = \sum_{el=1}^{no_{elm}} \int_{\partial\Omega_{el}} \bar{\mathbf{N}}^{T} \mathbf{t}_{L} \cdot \mathbf{n} \, d\partial\Omega = \sum_{el=1}^{no_{elm}} \sum_{i=1}^{no_{Nodes,el}} \sum_{MP=1}^{no_{MP,el}} \mathbf{N}^{T}(\boldsymbol{\xi}_{MP}) \, \mathbf{f}_{L,MP}^{ext,trac} \tag{4.95}$$

where $\mathbf{f}_{L,MP}^{ext}$ is the force stored in the material point due to distributed external forces applied at the boundary of the body, as described in Section 4.3.2.

The complete form of the external force is summarized below:

$$\mathbf{f}_{L}^{ext} = \sum_{el=1}^{no_{elm}} \sum_{i=1}^{no_{Nodes,el}} \sum_{MP=1}^{no_{MP,el}} \mathbf{N}^{T}(\boldsymbol{\xi}_{MP}) \, \mathbf{f}_{MP}^{ext} + \sum_{el=1}^{no_{elm}} \sum_{i=1}^{no_{Nodes,el}} \sum_{MP=1}^{no_{MP,el}} m_{MP} \mathbf{N}_{i}^{T}(\boldsymbol{\xi}_{MP}) \mathbf{g} \Omega_{MP} \tag{4.96}$$

### 4.5.5 Lumping procedure: Mass matrix and Drag matrix

To solve the system of equations (Eq. 4.105), the mass matrix has to be inverted. In practice, to simplify computations, a lumped mass matrix may be used instead of the consistent mass matrix given by Eq. 4.90. The lumped mass matrix is a diagonal matrix in which each entry $m_i$ is obtained by summing over the corresponding row of the consistent mass matrix. Matrix inversions become trivial, although the result of using a lumped mass matrix is some dissipation of kinetic energy that has been quantified by [11]. Using the property $\sum_{MP=1}^{no_{MP}} N_i(\boldsymbol{\xi}_{MP}) = 1$ it becomes

$$\bar{\mathbf{M}}_{L}^{lump} = \sum_{el=1}^{no_{elm}} \sum_{i=1}^{no_{Nodes,el}} \sum_{MP=1}^{no_{MP,el}} \mathbf{N}^{T}(\boldsymbol{\xi}_{MP}) \, m_{L,MP} \tag{4.97}$$

Hereinafter, the superscript lump is removed from the lumped mass matrix $\bar{\mathbf{M}}^{lump}$ to simplify the notation, and mass matrix always will refer to a lumped matrix.

In this study the 4-node tetrahedral element is used and the lumping procedure gives the following expression for the mass matrix $\bar{\mathbf{M}}_{L}$.

$$\bar{\mathbf{M}}_L = \sum_{el=1}^{n_{elm}} \mathbf{M}_{L,el} \tag{4.98}$$

$$\bar{\mathbf{M}}_{L,el} = \begin{bmatrix} \mathbf{m}_1 & \mathbf{0} & \mathbf{0} & ... & \mathbf{0} \\ \mathbf{0} & \mathbf{m}_2 & \mathbf{0} & ... & \mathbf{0} \\ \mathbf{0} & ... & ... & \mathbf{m}_i & \mathbf{0} \\ \mathbf{0} & \mathbf{0} & \mathbf{0} & ... & \mathbf{m}_{NodeEl} \end{bmatrix} \tag{4.99}$$

$$\mathbf{m}_i = \begin{bmatrix} m_i & 0 & 0 \\ 0 & m_i & 0 \\ 0 & 0 & m_i \end{bmatrix} \; ; \; \mathbf{0} = \begin{bmatrix} 0 & 0 & 0 \\ 0 & 0 & 0 \\ 0 & 0 & 0 \end{bmatrix} \tag{4.100}$$

$$m_i = \sum_{MP=1}^{no_{MP,el}} m_{L,MP} N_i(\xi_{MP}) \tag{4.101}$$

The same procedure is used to calculate the lumped mass matrix for the solid phase $\mathbf{M}_S$.

The drag force $\mathbf{f}^d$ can be written as follows

$$\mathbf{f}^d = \mathbf{Q}\,(\hat{\mathbf{v}}_L - \hat{\mathbf{v}}_S) \tag{4.102}$$

with

$$\mathbf{Q} = \int_\Omega \bar{\mathbf{N}}^T n \frac{\rho_L g}{k} \bar{\mathbf{N}}\, d\Omega$$

The lumping technique is also applied to the drag matrix $\mathbf{Q}$ as follows:

$$\mathbf{Q}^{lump} = \sum_{el=1}^{no_{elm}} \sum_{i=1}^{no_{Nodes,el}} \sum_{k=1}^{no_{int,el}} \mathbf{N}_i^T n_k \frac{\rho_L g}{k} |J_k| \tag{4.103}$$

Hereinafter, likewise for the mass matrix, the superscript lump is removed form the lumped drag matrix $\mathbf{Q}^{lump}$ to simplify the notation, and drag matrix always will be refereed to a lumped matrix. In this study the 4-node tetrahedral element is used and the lumping procedure gives the following compact expression:

$$\mathbf{Q} = \sum_{el=1}^{n_{elm}} \mathbf{Q}_{el} \; ; \; \mathbf{Q}_{el} = \begin{bmatrix} \mathbf{q}_1 & \mathbf{0} & \mathbf{0} & ... & \mathbf{0} \\ \mathbf{0} & \mathbf{q}_2 & \mathbf{0} & ... & \mathbf{0} \\ \mathbf{0} & ... & ... & \mathbf{q}_i & \mathbf{0} \\ \mathbf{0} & \mathbf{0} & \mathbf{0} & ... & \mathbf{q}_{NodeEl} \end{bmatrix}$$

$$\mathbf{q}_i = \begin{bmatrix} q_i & 0 & 0 \\ 0 & q_i & 0 \\ 0 & 0 & q_i \end{bmatrix} \; ; \; \mathbf{0} = \begin{bmatrix} 0 & 0 & 0 \\ 0 & 0 & 0 \\ 0 & 0 & 0 \end{bmatrix}$$

$$q_i = \sum_{k=1}^{no_{int,el}} n_k \frac{\rho_L g}{k} N_i(\xi_k) |J_k| W_k$$

where $no_{Nodes,el}$ and $no_{int,el}$ are respectively the number of nodes and integration points inside the element el, and $W_k$ is the weight factor (or integration weight) of the integration point k.

### 4.5.6 Numerical implementation

The discrete system of equations can be written as:

$$\mathbf{M}_L \hat{\mathbf{a}}_L^k = \mathbf{f}_L^{ext,k} - \mathbf{f}_L^{int,k} - \mathbf{f}^{d,k} \tag{4.104}$$

$$\mathbf{M}_S^t \hat{\mathbf{a}}_S^k = \mathbf{f}^{ext,k} - \mathbf{f}^{int,k} - \bar{\mathbf{M}}_L^k \hat{\mathbf{a}}_L^k \tag{4.105}$$

Note that in Eqs. 4.105 and 4.105 the subscript L and S denote that the quantity is referred to the fluid and water phase respectively; no subscript indicates that the quantity belongs to the mixture.

The Euler-Cromer scheme is used to integrate the equations in time. From Eq. 4.104 the fluid acceleration at time t is calculated and used to update the fluid velocity $\mathbf{v}_L^{t+\Delta t}$. The solid acceleration is calculated solving Eq. 4.105 and used to update the solid velocity $\mathbf{v}_S^{t+\Delta t}$. Incremental strains are calculated at the MP from the updated velocities, after that the constitutive relations are used to calculate the stresses and pore water pressure.

In the implementation used for this thesis only one set of MP, representing the solid phase is considered. This means that the MP store all the informations regarding the soild and the liquid phase, and their positions are updated according to the solid displacement.

### 4.5.7 Solution algorithm for single timestep

The initialization of MP explained in Section 4.3.2 is easily extended to the two-phase problem, then no more details are given in this Section.

The solution sequence of a single time step is described in the following:

1 The momentum equations for the fluid and the mixture are initialized by mapping the significative quantities from the MP to the mesh nodes. The procedure is similar to step 1 of the algorithm presented in Section 4.3.7.

2 Eq. 4.104 is solved for $\hat{\mathbf{a}}_L^t$

$$\hat{\mathbf{a}}_L^t = \mathbf{M}_L^{t,-1} \left[ \mathbf{f}_L^{ext,t} - \mathbf{f}_L^{int,t} - \mathbf{f}^{d,t} \right] \tag{4.106}$$

3 The acceleration vector $\mathbf{a}_S^t$ is calculated from Eq. 4.105 as:

$$\hat{\mathbf{a}}_S^t = \mathbf{M}_S^{t,-1} \left[ \mathbf{f}^{ext,t} - \mathbf{f}^{int,t} - \bar{\mathbf{M}}_L^t \mathbf{a}_L^t \right] \tag{4.107}$$

4 The velocities of the MPs are updated using nodal accelerations and shape functions:

$$\hat{\mathbf{v}}_{L,MP}^{t+\Delta t} = \hat{\mathbf{v}}_{L,MP}^t + \sum_{i=1}^{n_{en}} \Delta t N_i(\boldsymbol{\xi}_{MP}^t) \hat{\mathbf{a}}_{L,i}^t \tag{4.108}$$

$$\hat{\mathbf{v}}_{S,MP}^{t+\Delta t} = \hat{\mathbf{v}}_{S,MP}^t + \sum_{i=1}^{n_{en}} \Delta t N_i(\boldsymbol{\xi}_{MP}^t) \hat{\mathbf{a}}_{S,i}^t \tag{4.109}$$

5 The nodal velocities $\hat{\mathbf{v}}_L^{t+\Delta t}$ and $\hat{\mathbf{v}}_S^{t+\Delta t}$ are then calculated from the updated momentum solving the following equation

$$\mathbf{P}_{L,i}^{t+\Delta t} = \bar{\mathbf{M}}_L^t \hat{\mathbf{v}}_L^{t+\Delta t} \approx \sum_{MP=1}^{n_{MP}} m_{L,MP} \mathbf{N}^T(\boldsymbol{\xi}_{MP}^t) \hat{\mathbf{v}}_{L,MP}^{t+\Delta t} \tag{4.110}$$

$$\mathbf{P}_{S,i}^{t+\Delta t} = \mathbf{M}_S^t \hat{\mathbf{v}}_S^{t+\Delta t} \approx \sum_{MP=1}^{n_{MP}} m_{S,MP} \mathbf{N}^T(\boldsymbol{\xi}_{MP}^t) \hat{\mathbf{v}}_{S,MP}^{t+\Delta t} \tag{4.111}$$

6 Nodal velocities are integrated to get nodal incremental displacements

$$\Delta\hat{\mathbf{u}}_L^{t+\Delta t} = \Delta t\hat{\mathbf{v}}_L^{t+\Delta t}\ ;\ \Delta\hat{\mathbf{u}}_S^{t+\Delta t} = \Delta t\hat{\mathbf{v}}_S^{t+\Delta t} \tag{4.112}$$

7 Strains at MPs are calculated as

$$\Delta\varepsilon_{L,MP}^{t+\Delta t} = \mathbf{B}(\xi_{MP}^t)\hat{\mathbf{v}}_L^{t+\Delta t}\Delta t \tag{4.113}$$

$$\Delta\varepsilon_{S,MP}^{t+\Delta t} = \mathbf{B}(\xi_{MP}^t)\hat{\mathbf{v}}_S^{t+\Delta t}\Delta t \tag{4.114}$$

and stresses are updated according to a constitutive relation

8 Water pressures at the material points are updated as:

$$\Delta\bar{\varepsilon}_{L,MP}^{t+\Delta t} = \frac{1}{n_{MP}^t}\left[(1-n_{MP}^t)\Delta\varepsilon_{S,MP}^{t+\Delta t} + n_{MP}^t\Delta\varepsilon_{L,MP}^{t+\Delta t}\right] \tag{4.115}$$

$$p_{L,MP}^{t+\Delta t} \approx p_{L,MP}^t + K_{L,MP}\Delta\bar{\varepsilon}_{L,MP}^{t+\Delta t} \tag{4.116}$$

where $\boldsymbol{\delta} = \begin{bmatrix}1 & 1 & 1 & 0 & 0 & 0\end{bmatrix}$, $\Delta\varepsilon_{vol,S}$ and $\Delta\varepsilon_{vol,L}$ are the volumetric strain, i.e. $\Delta\varepsilon_{vol} = \Delta\varepsilon_{11} + \Delta\varepsilon_{22} + \Delta\varepsilon_{33}$, at the MP for the solid and liquid phase respectively.

9 The total stress is calculated as:

$$\boldsymbol{\sigma}_{MP}^{t+\Delta t} = \boldsymbol{\sigma}'^{t+\Delta t}_{MP} + \boldsymbol{\delta}p_{L,MP}^{t+\Delta t} \tag{4.117}$$

10 Volumes associated with MP are updated using the solid volumetric strain increment

$$\Omega_{MP}^{t+\Delta t} = (1 + \Delta\epsilon_{vol,S,MP}^{t+\Delta t}) \tag{4.118}$$

11 The positions of MP are updated using the displacements of the solid phase

$$\mathbf{x}_{MP}^{t+\Delta t} = \mathbf{x}_{MP}^t + \sum_{i=1}^{n_{no_{nodes}}} N_i(\xi_{MP}^t)\Delta\hat{\mathbf{u}}_{S,i}^{t+1} \tag{4.119}$$

12 The book-keeping is updated using the new position of particles

The reader should observe that, similarly to the one-phase solution procedure, MP velocity are calculated from nodal accelerations and nodal velocities are computed from the nodal momentum. This is called modified Lagrangian algorithm and allows to overcome the small mass problem.

## 4.6 Stability criterion: the Critical timestep

A numerical algorithm is stable and well posed when the numerical solution is maintained close to the exact one throughout the calculation, which means that the errors stay bounded. The stability of a numerical algorithm depends on the integration scheme. Explicit time integration schemes, such as the one presented above, are conditionally stable.

The Courant-Friedrichs-Levy condition is considered to obtain the critical time interval in order to achieve a stable solution.

### 4.6.1 Criterion for 1-phase-solid

The criterion to determine the critical timestep in case of 1-phase-solid simulation is the following

$$\Delta t_{cr} = \frac{L_{min}}{c} \; ; \; c = \sqrt{\frac{E_c}{\rho}} \tag{4.120}$$

where $E_c$ is the constrained modulus of the solid media. The length $L_{min}$ is the minimal length of the element and can be determined as the shortest distance from the side of the maximum area to the opposite node. The construction is shown in Figure 4.2.

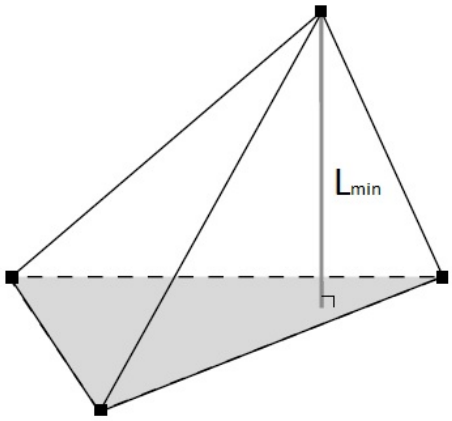


***Figure 4.2:*** *Minimum length* $L_{min}$ *for a tetrahedral element.*

### 4.6.2 Criterion for 1-phase-liquid

The criterion to determine the critical timestep in case of 1-phase-solid simulation is the following

$$\Delta t_{cr} = \frac{L_{min}}{c_L} \; ; \; c_L = \sqrt{\frac{K_L}{\rho_L}} \tag{4.121}$$

where $K_L$ is the bulk modulus of the water. The length $L_{min}$ is the minimal length of the element and can be determined as the shortest distance from the side of the maximum area to the opposite node. The construction is shown in Figure 4.2.

### 4.6.3 Criterion for 2-phase-coupled

The stability analysis of the 2-phase-coupled formulation is onerous; for this reason, a first simplified analysis was performed in [13] on a simplified formulation that is derived by assuming an incompressible pore fluid. Based on the eigenvalue analyses of a single linear finite element, it is observed that in addition to the CFL stability condition, the influence of the permeability must be included. The full stability criterion for the 2-phase-coupled formulation is represented by the following equation

$$\Delta t_{cr} = \min \left\{ \Delta t_{cr,1} ; \Delta t_{cr,2} \right\} \tag{4.122}$$

where

$$\Delta t_{cr,1} = m\frac{L_{min}}{c_1} \tag{4.123}$$

$$\Delta t_{cr,2} = \frac{2\tilde{\rho}k}{\rho_L g} \tag{4.124}$$

$$c_1 = \sqrt{\frac{E_c^u}{\rho}} \tag{4.125}$$

$$E_c^u = E_c + K_L/n \tag{4.126}$$

$$\rho = (1-n)\rho_S + n\rho_L \tag{4.127}$$

$$\tilde{\rho} = \rho + (\frac{1}{n} - 2)\rho_L \tag{4.128}$$

$E_c^u$ is the undrained constrained modulus of the saturated soil, $E_c$ is the laterally confined modulus of the solid skeleton and $K_L$ is the bulk modulus of the liquid. The length $L_{min}$ is the minimal length of the element and can be determined as the shortest distance from the side of the maximum area to the opposite node. The construction is shown in Figure 4.2.

It is worth noticing that $\Delta t_{cr,1}$ is a function of the size of the mesh, the stiffness, the porosity and the density of the material, while $\Delta t_{cr,2}$ is a function of the permeability, the porosity and the density. In many cases, the time step required to ensure the stability in low permeable soils can be smaller than the one required for high permeable soils, i.e. $\Delta t_{cr,2} < \Delta t_{cr,1}$.

The condition expressed by Eq. 4.122 can be improved and reformulated in the single equation [14]:

$$\Delta t_{cr} = \frac{-2a + \sqrt{4a^2 + 8(b + \sqrt{b^2 - 4c})}}{b + \sqrt{b^2 - 4c}} \tag{4.129}$$

The coefficients a, b and c are given by

$$a = \frac{n\rho g}{(1-n)\rho_S k} \tag{4.130}$$

$$b = \frac{4(n\rho K_L + (1-2n)\rho_L K_L + n\rho_L E_c)}{n(1-n)\rho_S \rho_L L_{min}} \tag{4.131}$$

$$c = \frac{16 E_c K_L}{(1-n)\rho_S \rho_L L_{min}} \tag{4.132}$$

## 4.7 4-node tetrahedral element

The isoparametric element used in this report is the 4-node tetrahedral. Figure 4.3 shows the element in the parent domain, in which the node number varies from 1 to 4, and in the global domain where the nodes numbers can vary arbitrarily depending on global mesh, and in this case number 11, 12, 13 and 14 are used as an example. One of the main feature of the isoparametric elements is that the shape functions in both parent and global domain are the same. Therefore, the coordinates of a point in the global domain are determined as follows

$$\mathbf{x}(\boldsymbol{\xi}, t) = \sum_{i=1}^{4} N_i(\boldsymbol{\xi})\, \mathbf{x}_i(t) \tag{4.133}$$

where $\boldsymbol{\xi}$ is the vector of the parent coordinate system which is written as follows

$$\boldsymbol{\xi} = [\xi_1 \;\; \xi_2 \;\; \xi_3]^T \tag{4.134}$$

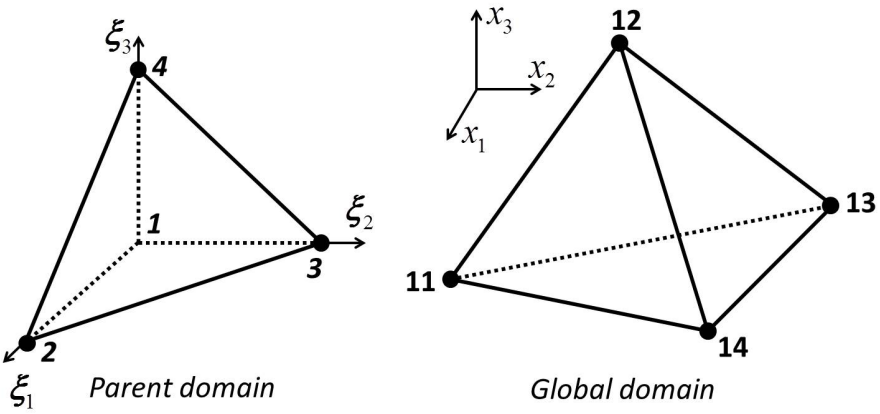


***Figure 4.3:*** *4-node tetrahedral element. Parent and Global domain.*

The shape function is defined in the parent domain, i.e. in the local coordinate system, as follows:

$$N_1(\boldsymbol{\xi}) = 1 - \xi_1 - \xi_2 - \xi_3 \tag{4.135}$$
$$N_2(\boldsymbol{\xi}) = \xi_1 \tag{4.136}$$
$$N_3(\boldsymbol{\xi}) = \xi_2 \tag{4.137}$$
$$N_4(\boldsymbol{\xi}) = \xi_3 \tag{4.138}$$

where the subscript $1, 2, 3$ or $4$ represents the node number in the parent domain.

Usually, the derivative of the shape function is also required to compute for instance the **B** matrix, which is needed to determine the internal forces of the system. The derivative is computed using the chain rule as follows

$$\begin{aligned}
\frac{\partial N_i(\boldsymbol{\xi})}{\partial \mathbf{x}_1} &= \frac{\partial N_i(\boldsymbol{\xi})}{\partial \boldsymbol{\xi}_1}\frac{\partial \boldsymbol{\xi}_1}{\partial \mathbf{x}_1} + \frac{\partial N_i(\boldsymbol{\xi})}{\partial \boldsymbol{\xi}_2}\frac{\partial \boldsymbol{\xi}_2}{\partial \mathbf{x}_1} + \frac{\partial N_i(\boldsymbol{\xi})}{\partial \boldsymbol{\xi}_3}\frac{\partial \boldsymbol{\xi}_3}{\partial \mathbf{x}_1} \\
\frac{\partial N_i(\boldsymbol{\xi})}{\partial \mathbf{x}_2} &= \frac{\partial N_i(\boldsymbol{\xi})}{\partial \boldsymbol{\xi}_1}\frac{\partial \boldsymbol{\xi}_1}{\partial \mathbf{x}_2} + \frac{\partial N_i(\boldsymbol{\xi})}{\partial \boldsymbol{\xi}_2}\frac{\partial \boldsymbol{\xi}_2}{\partial \mathbf{x}_2} + \frac{\partial N_i(\boldsymbol{\xi})}{\partial \boldsymbol{\xi}_3}\frac{\partial \boldsymbol{\xi}_3}{\partial \mathbf{x}_2} \\
\frac{\partial N_i(\boldsymbol{\xi})}{\partial \mathbf{x}_3} &= \frac{\partial N_i(\boldsymbol{\xi})}{\partial \boldsymbol{\xi}_1}\frac{\partial \boldsymbol{\xi}_1}{\partial \mathbf{x}_3} + \frac{\partial N_i(\boldsymbol{\xi})}{\partial \boldsymbol{\xi}_2}\frac{\partial \boldsymbol{\xi}_2}{\partial \mathbf{x}_3} + \frac{\partial N_i(\boldsymbol{\xi})}{\partial \boldsymbol{\xi}_3}\frac{\partial \boldsymbol{\xi}_3}{\partial \mathbf{x}_3}
\end{aligned} \tag{4.139}$$

The compact form can be written as follows

$$\begin{Bmatrix}
\frac{\partial N_i(\boldsymbol{\xi})}{\partial \mathbf{x}_1} \\
\frac{\partial N_i(\boldsymbol{\xi})}{\partial \mathbf{x}_2} \\
\frac{\partial N_i(\boldsymbol{\xi})}{\partial \mathbf{x}_3}
\end{Bmatrix} =
\begin{bmatrix}
\frac{\partial \boldsymbol{\xi}_1}{\partial \mathbf{x}_1} & \frac{\partial \boldsymbol{\xi}_2}{\partial \mathbf{x}_1} & \frac{\partial \boldsymbol{\xi}_3}{\partial \mathbf{x}_1} \\
\frac{\partial \boldsymbol{\xi}_1}{\partial \mathbf{x}_2} & \frac{\partial \boldsymbol{\xi}_2}{\partial \mathbf{x}_2} & \frac{\partial \boldsymbol{\xi}_3}{\partial \mathbf{x}_2} \\
\frac{\partial \boldsymbol{\xi}_1}{\partial \mathbf{x}_3} & \frac{\partial \boldsymbol{\xi}_2}{\partial \mathbf{x}_3} & \frac{\partial \boldsymbol{\xi}_3}{\partial \mathbf{x}_3}
\end{bmatrix}
\begin{Bmatrix}
\frac{\partial N_i(\boldsymbol{\xi})}{\partial \boldsymbol{\xi}_1} \\
\frac{\partial N_i(\boldsymbol{\xi})}{\partial \boldsymbol{\xi}_2} \\
\frac{\partial N_i(\boldsymbol{\xi})}{\partial \boldsymbol{\xi}_3}
\end{Bmatrix} \tag{4.140}$$

The derivatives of the natural coordinates $\boldsymbol{\xi}$ to the global coordinates $\mathbf{x}$ are not explicitly available. The (3x3) matrix in Eq.(4.140) is the inverse of the Jacobian matrix $\mathbf{J}$, which is defined as follows

$$\begin{bmatrix} \frac{\partial \boldsymbol{\xi}_1}{\partial \mathbf{x}_1} & \frac{\partial \boldsymbol{\xi}_2}{\partial \mathbf{x}_1} & \frac{\partial \boldsymbol{\xi}_3}{\partial \mathbf{x}_1} \\ \frac{\partial \boldsymbol{\xi}_1}{\partial \mathbf{x}_2} & \frac{\partial \boldsymbol{\xi}_2}{\partial \mathbf{x}_2} & \frac{\partial \boldsymbol{\xi}_3}{\partial \mathbf{x}_2} \\ \frac{\partial \boldsymbol{\xi}_1}{\partial \mathbf{x}_3} & \frac{\partial \boldsymbol{\xi}_2}{\partial \mathbf{x}_3} & \frac{\partial \boldsymbol{\xi}_3}{\partial \mathbf{x}_3} \end{bmatrix} = \mathbf{J}^{-1} = \begin{bmatrix} \frac{\partial \mathbf{x}_1}{\partial \boldsymbol{\xi}_1} & \frac{\partial \mathbf{x}_1}{\partial \boldsymbol{\xi}_2} & \frac{\partial \mathbf{x}_1}{\partial \boldsymbol{\xi}_3} \\ \frac{\partial \mathbf{x}_2}{\partial \boldsymbol{\xi}_1} & \frac{\partial \mathbf{x}_2}{\partial \boldsymbol{\xi}_2} & \frac{\partial \mathbf{x}_2}{\partial \boldsymbol{\xi}_3} \\ \frac{\partial \mathbf{x}_3}{\partial \boldsymbol{\xi}_1} & \frac{\partial \mathbf{x}_3}{\partial \boldsymbol{\xi}_2} & \frac{\partial \mathbf{x}_3}{\partial \boldsymbol{\xi}_3} \end{bmatrix}^{-1} \tag{4.141}$$

# 5 The boundary conditions

The application of boundary conditions is a subject rarely discussed in the literature of the material point method. In this Chapter, the different types of boundary conditions that can be found in a mechanical problem are presented.

From a numerical point of view, two kinds of boundary conditions can be distinguished: natural and essential. On the one hand, essential boundary conditions are imposed directly on the solution. In this way, degrees of freedom are directly eliminated from the system of equations. Dirichlet conditions are an example. On the other hand, natural boundary conditions are imposed on a secondary variable, such as in Newman or Newton (Robin) conditions.

The boundary conditions required in a mechanical problem are summarized in Table 5.1. Those are prescribed traction and prescribed velocity, which correspond to natural and essential conditions respectively. In the numerical implementation, prescribed traction is included in the weak form of the governing equations, while calculated velocities are directly overwritten by the prescribed values.

***Table 5.1:*** *Types of boundary conditions in a mechanical problem.*

| Essential | Natural |
|---|---|
| Prescribed solid velocity | Prescribed traction |

It is commonly accepted that boundary conditions are specified at the nodes of the mesh [15, 16]. This idea makes sense considering that the governing equations are solved in the computational grid, and consequently the MPM formulation persists almost identical to that used in the FEM.

The problem of applying the boundary conditions at the nodes appears when a moving boundary is considered. In these cases, the boundary condition has to move attached to the body. However, in the standard MPM formulation, the computational mesh remains constant. Therefore, in such cases, the boundary condition should be carried by the material points.

This way of handling the boundary conditions to solve the issue of movement leads to some inaccuracies, specially in natural conditions. If the boundary condition is applied on a material point, this condition has to be distributed all over the nodes of the element to solve the system of equation. If a material point is affected by a moving boundary condition, the element containing the point becomes part of the contour. Then, the contour has an equivalent thickness of the size of the element and the boundary condition is spread affecting all material points within the cell, even those which are not at the boundary. To minimize numerical errors, it is recommended to use a fine mesh.

Another difficulty of moving boundaries appears when external traction has not a prescribed direction. This means that if the shape of the contour changes, the direction of the applied condition has to be updated during the calculation. This is an expensive procedure, in which the normal vector must be calculated at every time step.

In Figure 5.1 a very simple problem is presented. It shows the movement of a beam that is fixed at one end and subjected to a vertical force F at the opposite end. In this example the fixity can be understood as an essential boundary condition in which the prescribed velocity is zero. Because it remain motionless, it can be applied at the nodes. On the other hand, the vertical force is a natural boundary condition which moves attached to the beam, therefore it

should be carried by the material points.

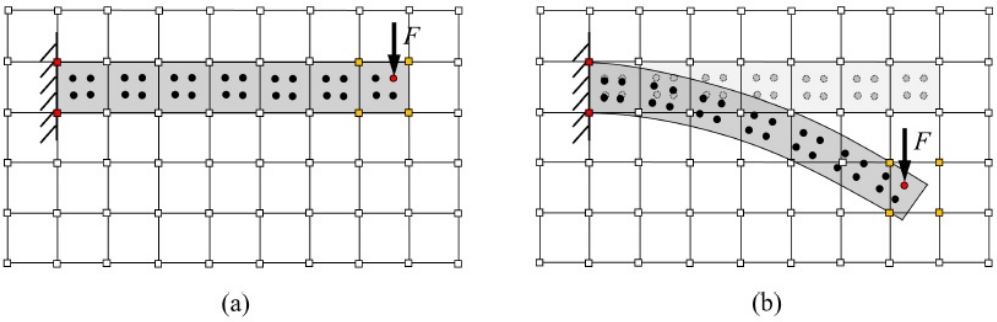


***Figure 5.1:*** *Problem of a beam subjected to a vertical force at one end and embedded at the other one. (a) Initial discretization; (b) final discretization. The boundary conditions are carried in those nodes and material points colored in red. Yellow nodes are affected by the moving boundary condition although it is not stored in them [from [5]].*

## 5.1 Zero kinematic boundary conditions

Such boundary conditions are easy to apply in MPM. Zero kinematic boundary conditions are applied in a way that is identical to that of standard Lagrangian FEM. Special attention should however be paid when applying those conditions in the framework of MPM, that is they also have to be applied on those boundary nodes that might become active during computations. This ensures that, when a previously inactive node becomes active during computations, zero prescribed kinematic boundary conditions at this node must be applied (activated). Figure 5.2 illustrates such a situation. Regarding zero traction boundary conditions, they are automatically enforced to be satisfied by the solution of equations of motion.

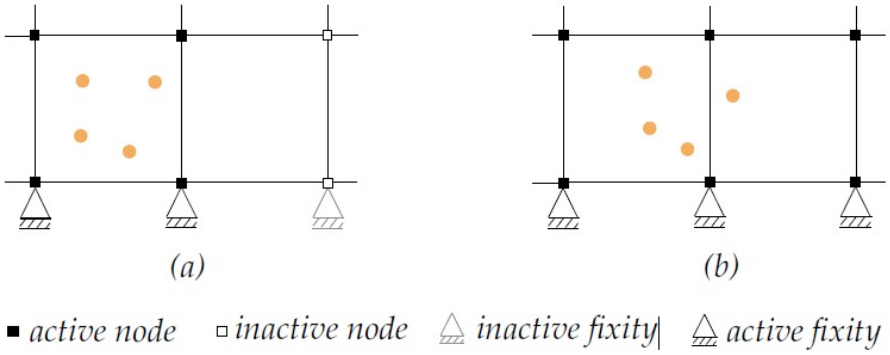


***Figure 5.2:*** *Kinematic boundary conditions are prescribed at the active and inactive nodes (a) inactive fixity (b) active fixity. [from. Al-Kafaij 2013]*

## 5.2 Traction boundary conditions

The external forces applied at the traction boundary are mapped to the material points located next to the element border, also called boundary material points. These MP carry surface traction throughout the computations. Considering a tetrahedral element, the traction vector $\tau_e$ applied at the triangular surface is interpolated from the nodes of this surface to the boundary MP. See figure 5.3. Hence, the traction at boundary material point MP is

$$\tau_e(\mathbf{x}_{MP}) \approx \sum_{i=1}^{n_{tri}} N_i(\xi_{MP})\tau_e(\mathbf{x}_i) \tag{5.1}$$

where $N_i$ is the shape function of node i of the triangular surface element and $\xi_{MP}$ are the coordinates of the boundary material point MP inside the parent triangular element. These coordinates simply represent the projection of the MP on the triangular surface element. The traction force vector $\mathbf{f}_{MP}^{trac}$ is then

$$\mathbf{f}_{MP}^{trac} = \tau_e(\mathbf{x}_{MP})\frac{S_e}{n_{ebMP}} = \frac{S_e}{n_{ebMP}}\sum_{i=1}^{n_{tri}} N_i(\xi_{MP})\tau_e(\mathbf{x}_i) \tag{5.2}$$

in which $n_{ebMP}$ denotes the number of boundary MP located next to the loaded surface. This force vector keep the same direction and intensity throughout the calculation.

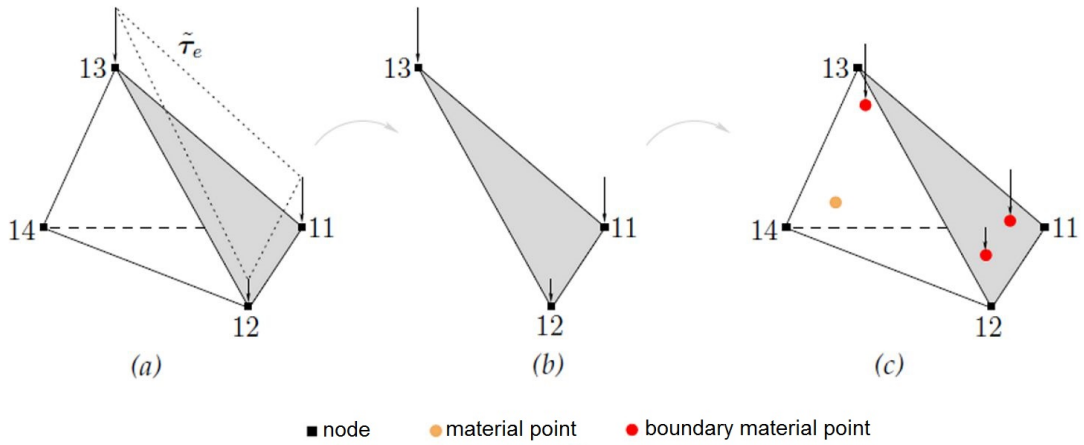


***Figure 5.3:*** *Traction is mapped from a boundary particle to all nodes of the element. [from. Al-Kafaij 2013]*

During the simulation the boundary particles move throughout the computational mesh, and a way to treat such tractions during the MPM simulation is to map them from boundary material points to all nodes of the element where a boundary particle is located, see Figure 5.4. Such mapping procedure is carried out according to the following equation.

$$\mathbf{f}^{tract} = \sum_{el=1}^{no_{el}}\sum_{MP=1}^{no_{MP,el}} \mathbf{N}^T(\xi_{MP})\mathbf{f}_{MP}^{trac} \tag{5.3}$$

The disadvantage of this way of dealing with surface tractions is that the effect of the surface force is distributed over the layer of elements that borders the boundary. To reduce such smearing error, the thickness of the elements along the boundary should be small.

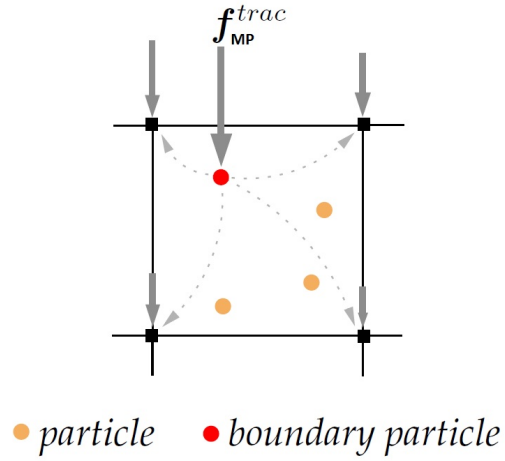


***Figure 5.4:*** *Traction is mapped from a boundary particle to all nodes of the element. [from. Al-Kafaij 2013]*

# 6 Advanced concepts

## 6.1 Introduction

Some additional features are described in this chapter. The contact algorithm first, then the local damping for both 1-phase and 2-phase material, and then the mass scaling procedure for quasi-static problems are initially discussed. Lastly, the strategies for mitigation of pathological locking for low order elements is also examined.

## 6.2 Contact problems

Problems of soil-structure interaction are common in geotechnical engineering. MPM is naturally capable of handling non-slip contact between different bodies, indeed inter-penetration cannot occur because the bodies' velocities belong to the same vector field. However, when continuum bodies come into contact, in most cases frictional sliding occurs at the contact surface. To simulate such a sliding interaction a specific contact algorithm that allows relative motion at the interface between contacting bodies is required.

In this section the contact algorithm proposed by [17] is presented as well as its extension to the adhesive contact. The advantage of this algorithm is that it does not require any special interface element. It proved to be efficient in modeling interaction between solid bodies as well as shearing in granular materials.

The adhesive type of contact is well suited to simulate soil-structure interaction in case of cohesive soil under undrained conditions. Indeed, in this case the tangential force cannot exceed the undrained shear strength.

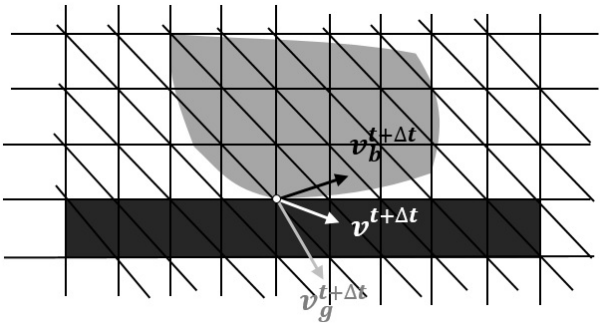


***Figure 6.1:*** *Example of two bodies in contact.*

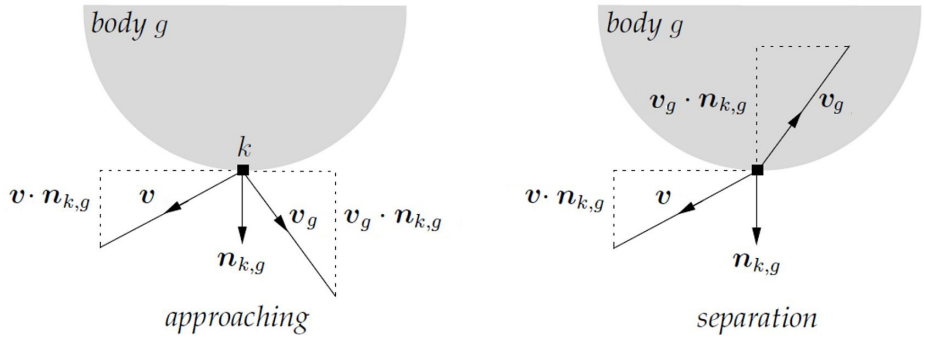


***Figure 6.2:*** *Cases of approaching bodies (left) and separating bodies (right) (Al-Kafaji 2013).*

### 6.2.1 Formulation

The contact algorithm used in Anura3Dcan be considered as a predictor-corrector scheme, in which the velocity is predicted from the solution of each body separately and then corrected using the velocity of the coupled bodies following the contact law.

Consider body *g* (gray in Fig. 6.1) and body *b* (black in Fig. 6.1), which are in contact at time t. The procedure starts with the initialization of the equation of motion (Eq. 4.20) for each body separately, as well as for the combined system.

The nodal accelerations for each body and the combined system are calculated solving the momentum equations and then used to predict the nodal velocities at time t + $\Delta$t as follows:

$$\mathbf{v}_g^{t+\Delta t} = \mathbf{v}_g^t + \Delta t \mathbf{a}_g^t \tag{6.1}$$

$$\mathbf{v}_b^{t+\Delta t} = \mathbf{v}_b^t + \Delta t \mathbf{a}_b^t \tag{6.2}$$

$$\mathbf{v}^{t+\Delta t} = \mathbf{v}^t + \Delta t \mathbf{a}^t \tag{6.3}$$

In this code, the contact surface is predefined by the user during the pre-processing phase. For each contact node, the algorithm proceeds with checking if the bodies are approaching or separating. This is done by comparing the normal component of the single body velocity with the normal component of the combined bodies velocity. Hence, the following two cases are possible:

$$(\mathbf{v}_g^{t+\Delta t} - \mathbf{v}^{t+\Delta t}) \cdot \mathbf{n}_k^t > 0 \quad \Rightarrow \quad \text{approaching}$$

$$(\mathbf{v}_g^{t+\Delta t} - \mathbf{v}^{t+\Delta t}) \cdot \mathbf{n}_k^t < 0 \quad \Rightarrow \quad \text{separating}$$

where $\mathbf{n}_k^t$ is the unit outward normal to body g at node k. The algorithm allows for free separation, i.e. no correction is required in this case and each body moves with the single body velocity $\mathbf{v}_{g(b)}^{t+\Delta t}$. If the bodies are approaching, than we need to check whether sliding occurs.

The predicted relative normal and tangential velocities at an approaching contact node can be respectively written as:

$$\mathbf{v}_{norm}^{t+\Delta t} = \left[ \left( \mathbf{v}_g^{t+\Delta t} - \mathbf{v}^{t+\Delta t} \right) \cdot \mathbf{n}_k^t \right] \mathbf{n}_k^t \tag{6.4}$$

$$\mathbf{v}_{tan}^{t+\Delta t} = \mathbf{n}_k^t \times \left[ \left( \mathbf{v}_g^{t+\Delta t} - \mathbf{v}^{t+\Delta t} \right) \times \mathbf{n}_k^t \right] \tag{6.5}$$

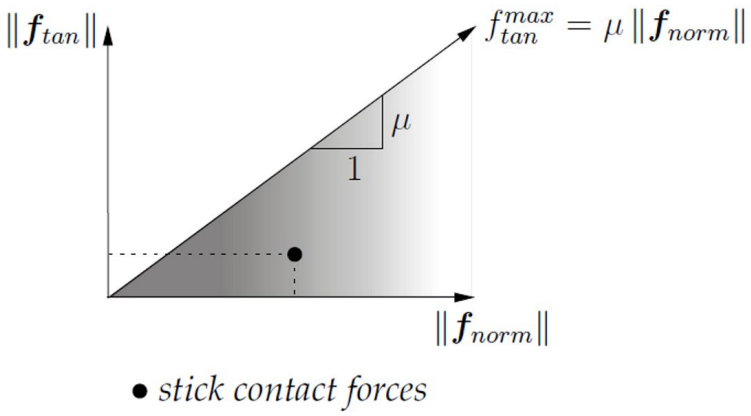


***Figure 6.3:*** *Contact forces for the stick case (Al-Kafaji 2013).*

These components can be used to predict the contact forces at the node as:

$$\mathbf{f}_{norm}^{t+\Delta t} = \frac{m_{k,g}^{t}}{\Delta t}\mathbf{v}_{norm}^{t+\Delta t} \tag{6.6}$$

$$\mathbf{f}_{tan}^{t+\Delta t} = \frac{m_{k,g}^{t}}{\Delta t}\mathbf{v}_{tan}^{t+\Delta t} \tag{6.7}$$

where $m_{k,g}^{t}$ is the nodal mass integrated from MP of body g.

The maximum tangential force is:

$$f_{tan}^{max,t+\Delta t} = f_{adh}^{t+\Delta t} + \mu \left|\mathbf{f}_{tan}^{t+\Delta t}\right| \tag{6.8}$$

where $f_{adh}^{t+\Delta t}$ is the adhesive force at the contact and $\mu$ is the friction coefficient.

Depending on the magnitude of the predicted contact forces we can distinguish between stick and slip contact:

$$\text{If} \quad \left|\mathbf{f}_{tan}^{t+\Delta t}\right| < f_{tan}^{max,t+\Delta t} \quad \Rightarrow \quad \text{stick contact}$$

$$\text{If} \quad \left|\mathbf{f}_{tan}^{t+\Delta t}\right| > f_{tan}^{max,t+\Delta t} \quad \Rightarrow \quad \text{slip contact}$$

In the first case, i.e. the bodies stick to each others, no correction is required and the velocity corresponds to $\mathbf{v}^{t+\Delta t}$. In the second case, i.e. the bodies are sliding one respect to the other, the velocity needs to be corrected in such a way that no inter-penetration is allowed and the magnitude of the tangential force respect Eq. 6.8.

The predicted single body velocity $\mathbf{v}_{g}^{t+\Delta t}$ is corrected to a new velocity $\tilde{\mathbf{v}}_{k,g}^{t+\Delta t}$ such that the normal component coincide with the normal component of the combined bodies velocity, i.e.,

$$\tilde{\mathbf{v}}_{g}^{t+\Delta t} \cdot \mathbf{n}_{k}^{t} = \mathbf{v}^{t+\Delta t} \cdot \mathbf{n}_{k}^{t} \tag{6.9}$$

which can also be written as

$$\tilde{\mathbf{v}}_{g}^{t+\Delta t} = \mathbf{v}_{g}^{t+\Delta t} + \mathbf{c}_{norm}^{t+\Delta t} \tag{6.10}$$

where

$$\mathbf{c}_{norm}^{t+\Delta t} = -\left[\left(\mathbf{v}_{g}^{t+\Delta t} - \mathbf{v}^{t+\Delta t}\right) \cdot \mathbf{n}_{k}^{t}\right]\mathbf{n}_{k}^{t} \tag{6.11}$$

is the correction of the normal component of the predicted velocity.

This correction is equivalent to apply the following normal contact force:

$$\tilde{\mathbf{f}}_{norm}^{t+\Delta t} = \frac{m_{k,g}^{t}}{\Delta t}\mathbf{c}_{norm}^{t+\Delta t} \tag{6.12}$$

When sliding occurs, the maximum tangential contact force assumes the expression:

$$\tilde{\mathbf{f}}_{tan}^{t+\Delta t} = f_{tan}^{max,t+\Delta t}\mathbf{t} \tag{6.13}$$

with **t** being a unit vector indicating the direction of the tangent.

Substituting Eq. 6.8 into Eq. 6.13 we get:

$$\tilde{\mathbf{f}}_{tan}^{t+\Delta t} = \left(f_{adh}^{t+\Delta t} + \mu \left|\mathbf{f}_{norm}^{t+\Delta t}\right|\right)\mathbf{t} \tag{6.14}$$

The total contact force is:

$$\tilde{\mathbf{f}}_{cont}^{t+\Delta t} = \tilde{\mathbf{f}}_{tan}^{t+\Delta t} + \tilde{\mathbf{f}}_{norm}^{t+\Delta t} \tag{6.15}$$

which is used to correct the velocity as:

$$\tilde{\mathbf{v}}_{g}^{t+\Delta t} = \mathbf{v}_{g}^{t+\Delta t} + \frac{\tilde{\mathbf{f}}_{cont}^{t+\Delta t}}{m_{k,g}^{t}}\Delta t \tag{6.16}$$

It can also be written as:

$$\tilde{\mathbf{v}}_{g}^{t+\Delta t} = \mathbf{v}_{g}^{t+\Delta t} + \mathbf{c}_{norm}^{t+\Delta t} + \mathbf{c}_{tan}^{t+\Delta t} \tag{6.17}$$

where the correction for the tangential component assumes the form:

$$\mathbf{c}_{tan}^{t+\Delta t} = \frac{\Delta t}{m_{k,g}^{t}}\left(f_{adh}^{t+\Delta t} + \mu \left|\mathbf{f}_{norm}^{t+\Delta t}\right|\right)\mathbf{t} \tag{6.18}$$

The force introduced by the adhesion a can be expressed as;

$$f_{adh}^{t+\Delta t} = aA_{k}^{t} \tag{6.19}$$

where $A_k^t$ is the contact area associated with the node k. It is integrated from the contact elements that share node k.

Substituting Eqs. 6.19 and 6.12 in Eq. 6.18, the corrected velocity can be written as:

$$\tilde{\mathbf{v}}_{g}^{t+\Delta t} = \mathbf{v}_{g}^{t+\Delta t} - \left[\left(\mathbf{v}_{g}^{t+\Delta t} - \mathbf{v}^{t+\Delta t}\right)\cdot\mathbf{n}_{k}^{t}\right]\mathbf{n}_{k}^{t} - \left\{\left[\left(\mathbf{v}_{g}^{t+\Delta t} - \mathbf{v}^{t+\Delta t}\right)\cdot\mathbf{n}_{k}^{t}\right]\mu + \frac{aA_{k}^{t}\Delta t}{m_{k,g}^{t}}\right\}\mathbf{t} \tag{6.20}$$

Fig. 6.4 illustrates with a flow chart the main steps of the implemented contact algorithm.

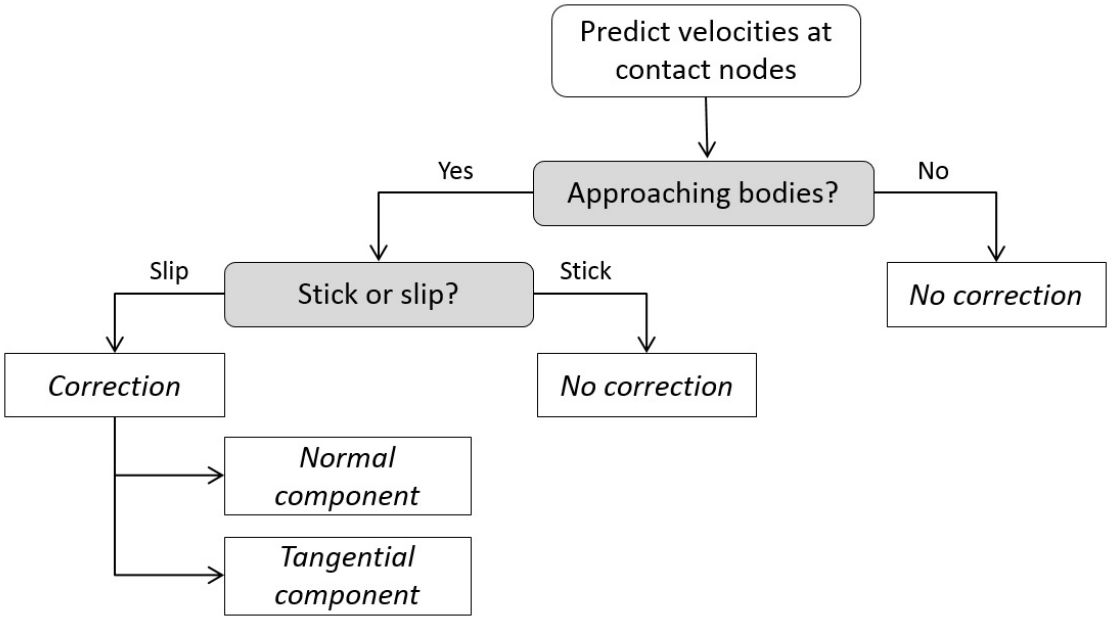


***Figure 6.4:*** *Flow chart illustrating the contact algorithm.*

Having calculated the velocity of the contact node k at time t + $\Delta$t, the corrected acceleration vector at the node must be recalculated as:

$$\tilde{\mathbf{a}}_g^t = \frac{\tilde{\mathbf{v}}_g^{t+\Delta t} - \mathbf{v}_g^t}{\Delta t} \tag{6.21}$$

This corrected acceleration is used to update the MP velocity according to the algorithm presented previously. It should be remarked that the contact algorithm is applied between the Lagrangian phase and the convective phase. Indeed the nodal velocities are first predicted in the Lagrangian phase, then the corrected nodal velocities and accelerations are computed by the contact algorithm and these new values of nodal accelerations are used to compute the velocities at the MP in the convective phase. The same procedure explained here for body g must be applied to body b.

## 6.3 Local damping

Natural dynamic systems contain some degree of damping of the vibration energy within the system; otherwise, the system would oscillate indefinitely when subjected to driving forces. Damping is due, in part, to energy loss as a result of internal friction in the intact material and slippage along interfaces, if these are present.

### 6.3.1 Single-phase problem

For a dynamic analysis, the damping in the numerical simulation should reproduce in magnitude and form the energy losses in the natural system when subjected to a dynamic loading. In soil and rock, natural damping is mainly hysteretic, i.e. independent of frequency, see [18] and [19]. This type of damping is difficult to reproduce numerically. However, if a constitutive model is found that contains an adequate representation of the hysteresis that occurs in a real material, then no additional damping would be necessary [20].

Rayleigh damping is commonly used to provide damping that is approximately frequency-independent over a restricted range of frequencies. However, this kind of damping introduces body forces that retard the steady state collapse and might influence the mode of failure [21]. [22] describes a local non-viscous damping to overcome the difficulty associated with the viscous damping.

An alternative to Rayleigh damping is the so-called local damping. The local damping force is proportional to the out of balance force $f = f^{ext} - f^{int}$ and acts opposite to the direction of the velocity. For any degree-of-freedom in the considered system, the local damping can be described as follows

$$ma = f + f^{damp} \tag{6.22}$$

where

$$f^{damp} = -\alpha \left|f\right| \frac{v}{\left|v\right|} \tag{6.23}$$

is the damping force at the considered degree of freedom. The dimensionless parameter $\alpha$ is called local damping factor.

### 6.3.2 Two-phase problem

In the two-phase formulation the fluid and the solid phase are damped separately. At any degree of freedom the momentum equation for the water assumes the form:

$$m_w a_w = f_w^{trac} + f_w^{grav} - f_w^{int} - f_w^{drag} + f_w^{damp} \tag{6.24}$$

if $f_w = f_w^{trac} + f_w^{grav} - f_w^{int}$ is the unbalanced force for the water, the damping force for the water can be written as:

$$f_w^{damp} = -\alpha_w \left|f_w\right| \frac{w}{\left|w\right|} \tag{6.25}$$

The momentum equation for the mixture is:

$$m_s a_s = -\bar{m}_w a_w + f^{trac} + f^{grav} - f^{int} + f^{damp} \tag{6.26}$$

where

$$f^{damp} = f_s^{damp} + f_w^{damp} \tag{6.27}$$

The out of balance force for the solid phase is $f = f^{trac} + f^{grav} - f^{int}$, hence the damping force for the solid can be written as:

$$f_s^{damp} = -\alpha_s \left|f - f_w\right| \frac{v}{\left|v\right|} \tag{6.28}$$

In this thesis the local damping factor for the fluid ($\alpha_w$) and the solid ($\alpha_s$) phase always assume the same value.

Local damping was originally designed for static simulations. However, it has some characteristics that make it attractive for dynamic simulations if proper values of the damping coefficient are used. In quasi-static problems high value of $\alpha$, i.e. 0.7-0.8, can be used to accelerate convergence. In slow-process problems a small value of $\alpha$, i.e. 0.05-0.15, can simulate natural energy dissipation of the material, if it is not taken into account by the constitutive model. Local damping should not be used or used only with high care in highly dynamic problem, where wave propagation is of great importance.

## 6.4 Convergence to static equilibrium

The dynamic MPM can also be adopted to model quasi-static problems, therefore, a criteria for the detection of the static equilibrium is required. The static equilibrium is reached when both the out-of-balance forces and the kinetic energy of the system vanish. The out-of-balance convergence criterion is usually adopted in quasi-static formulation to detect equilibrium.

Let us define a dimensionless force ratio F as

$$F = \frac{\|F_{ext} - F_{int}\|}{\|F_{ext}\|} \tag{6.29}$$

Together with the out-of-balance criterion, we adopt another criterion to ensure that the kinetic energy of the system vanishes. Let us define E, a dimensionless energy ratio, as

$$E = \frac{KE}{W_{ext}} \tag{6.30}$$

where KE denotes the kinetic energy of the system and $W_{ext}$ is the work induced by the external forces. The system is assumed to have reached static equilibrium when F and E reach a pre-defined tolerance.

## 6.5 Mass scaling for quasi-static problems

The simulation of quasi-static or slow-process problems with a dynamic explicit code can require high computational effort because the time step size is bounded by the stability condition. However, if the inertia effect is negligible, then the time step size can be artificially increased by scaling the density. Introducing the mass scaling factor $\beta$, the critical time step size increases by a factor $\sqrt{\beta}$. Indeed:

$$\Delta t^{\beta}_{crit} = \frac{l_e}{\sqrt{\frac{E_c}{\beta\rho}}} = \sqrt{\beta}\Delta t^{1}_{crit} \tag{6.31}$$

where $\Delta t^{1}_{crit}$ is the critical time step for $\beta = 1$, i.e. no mass scaling is applied.

Mass scaling is a very useful technique to improve computational efficiency of dynamic codes in simulating quasi-static ans slow-process motion. However, sensitivity analysis are necessary to calibrate the mass scaling factor in slow process problems, indeed extremely high values of $\beta$ can significantly effect the result.

## 6.6 Cell-crossing instability and *MPM-MIXED*

The classical MPM approach suffers from a "cell-crossing instability" for problems involving large displacements. Whenever material points cross boundaries of any element in the computational background grid, an unphysical unbalance force appears at the nodes that are shared between previous and new elements of that crossing points. The explanation for that is the lack of smoothness of the nodal shape functions used in the interpolation of information between grid and material points. The shape functions are linear $C^0$, which means that the gradients of the shape functions within the element are constant but they are discontinuous at the element borders (they change the sign). These gradients are used in the calculation of the nodal internal forces as described in Section 4.3.3. Therefore, when one material point

crosses a border, the internal forces of those involved nodes suffer an unphysical instability due to a jump discontinuity in the gradient of linear shape functions.

In this code there is a procedure to mitigate the cell-crossing instability. This simple procedure arises from calculating the stress of each element as a constant value that corresponds to the average of the stresses of the material points that at time $t^k$ are located within the element. Based on that, Gauss integration is adopted to determine the internal forces (as in FEM), in which a single point with an averaged stress $\boldsymbol{\sigma}_{av}$ is considered in each element. The stress averaging is calculated according to the following expression (Eq. 6.32), where $no_{MP,el}$ is the number of material points within the element, and $\boldsymbol{\sigma}_{MP}$ and $\Omega_{MP}$ are the stress and the volume of a material point, respectively.

$$\boldsymbol{\sigma}_{av} = \frac{\sum_{MP=1}^{no_{MP,el}} \boldsymbol{\sigma}_{MP}\, \Omega_{MP}}{\sum_{MP=1}^{no_{MP,el}} \Omega_{MP}} \tag{6.32}$$

The calculation of the internal forces by means of the Gauss point integration is only considered in the elements located in the interior of the continuum. The Gauss point integration is also used for the elements located at the boundaries only if the following condition is fulfilled:

$$\sum_{MP=1}^{no_{MP,el}} \Omega_{MP} > F_{fill}\, \Omega_{el} \tag{6.33}$$

in which the factor $F_{fill}$ is set to 0.9. It the aforementioned condition (Eq. (6.33)) is not fulfilled, the internal force in the boundary elements is calculated with the classic MPM procedure. This is a mixed approach which uses material points (MP) and Gauss points to calculate the internal force, and in the current code is named *MPM-MIXED*.

## 6.7 Patological locking in low order elements

### 6.7.1 Strain smoothing procedure

The formulation of the MPM is very close to the FEM in many aspects. At some point, this similarity is beneficial because most of the existing knowledge can be transferred to the MPM. However, several shortcomings associated with the FEM have been inherited by the MPM. Probably one of the most important limitation is the kinematic locking that can occur due to the linearity of the traditional shape functions constructed on the computational mesh. Difficulties arise when determining the displacement field for a nearly incompressible solid.

As a simple example of this phenomenon, consider Fig. 6.5. Element $e_1$, in Fig. 6.5a, is defined by nodes 1 and 2 on the x axis, and node 3 on the y axis. The area of the triangular element must remain constant if it is incompressible. If nodes 1 and 2 are fixed, $y_3$ must remain constant and $u_y^3 = 0$. Therefore, the remaining degree of freedom is the horizontal displacement $u_x^3$. Similarly, the only remaining degree of freedom in the element $e_2$ (Fig. 6.5b) defined by nodes 4, 5, and 6, is the vertical displacement $u_y^5$. Two triangles may be assembled, see Fig. 6.5c. Since incompressibility for element $e_1$ requires $u_y^3 = 0$ and incompressibility for element $e_2$ requires $u_x^3 = 0$, node 3 cannot move, and both elements are completely locked up. With nodes 1 through 4 locked up, the nodes for elements 3, 4, 5, 6, 7 and 8 will also be locked (Fig. 6.5c). Such locking usually propagates throughout the entire mesh yielding an unrealistic stiff response and an erroneous velocity field.

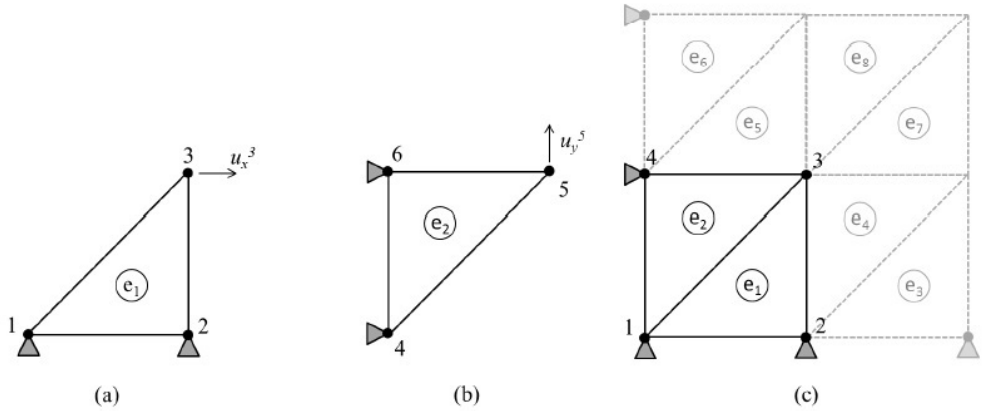


***Figure 6.5:*** *A pathological case of volumetric locking in triangular elements. Degrees of freedom are indicated.*

Several anti-locking approaches have been presented by different authors to mitigate this numerical problem associated with the linear shape functions [23, 24]. In this work, the Nodal Mixed Discretization (NMD) technique for linear tetrahedra elements presented by [24] has been used to mitigate the over-stiff behaviour. This procedure has showed effectiveness in mitigating the locking associated with (near) incompressible deformations [10]. In this technique, the element volumetric behaviour is averaged over the elements sharing its nodes via a least squares smoothing process. The effect of applying the NMD scheme is to increase the number of degrees of freedom per element. Being $\dot{\varepsilon}$ the strain rate of an element calculated from nodal velocities, it can be divided into deviatoric $\dot{\mathbf{e}}$ and volumetric $\dot{\varepsilon}_{\text{vol}}$ components as

$$\dot{\varepsilon} = \dot{\mathbf{e}} + \dot{\varepsilon}_{\text{vol}}\boldsymbol{\delta} \tag{6.34}$$

where $\boldsymbol{\delta} = (1, 1, 1, 0, 0, 0)^{\text{T}}$.

The volumetric strain rate for a node i, can be defined as weighted average of the surrounding element values $\dot{\varepsilon}_{\text{vol,e}}$ with the following equation:

$$\dot{\varepsilon}_{\text{vol,i}} = \frac{\sum_{\text{el}=1}^{\text{no}_{\text{el,i}}} \dot{\varepsilon}_{\text{vol,el}}\Omega_{\text{el}}}{\sum_{\text{el}=1}^{\text{no}_{\text{el,i}}} \Omega_{\text{el}}} \tag{6.35}$$

where $\text{no}_{\text{el,i}}$ are the elements surrounding the node i, and $\Omega_{\text{el}}$ is the volume of the element el.

Then, a mean value for the element, $\overline{\dot{\varepsilon}}_{\text{vol}}$ is calculated by taking the average of nodal quantities as

$$\overline{\dot{\varepsilon}}_{\text{vol}} = \frac{1}{\text{no}_{\text{node,el}}} \sum_{\text{i}=1}^{\text{no}_{\text{node,el}}} \dot{\varepsilon}_{\text{vol,i}} \tag{6.36}$$

where $\text{no}_{\text{node,el}}$ is the number of nodes in an element.

Finally, the element strain rates is redefined by superposition of the deviatoric part and the volumetric average as

$$\dot{\varepsilon} = \dot{\mathbf{e}} + \overline{\dot{\varepsilon}}_{\text{vol}}\boldsymbol{\delta} \tag{6.37}$$

## 6.8 Liquid free surface detection

The free surface problem is an important topic in coastal applications and many engineering problems. The expression for free surface is due to the contact of two fluids having different densities where free surface is developed at the interface. It is important to detect this surface properly. In most applications where single fluid flow is involved, a fluid experiences a free surface as exposed to the atmospheric pressure, where the air pressure corresponds to gauge pressure. The important feature of this type of problems that the shape of the surface is unknown, a priori, as it depends on the developed flow.

In MPM, mass density field can be evaluated at nodes each time increment. In this approach, the density field is represented at the grid nodes using the following formula

$$\rho_{L,i} = \frac{\sum_{el=1}^{no_{el,i}} \sum_{MP=1}^{no_{MP,el}} N_i(\xi_{MP})\, m_{MP}}{\sum_{el=1}^{no_{el,i}} \frac{\Omega_{el}}{no_{nodes,el}}} \tag{6.38}$$

Important to highlight here that the denominator of Eq. 6.38 involves only the non–empty elements, so that the density if approximated properly.

Consequently, the density at any location **x** inside elements can be interpolated using

$$\tilde{\rho}_{L,MP} = \sum_{i=1}^{no_{node,el}} N_i(\xi_{MP})\, \rho_{L,i} \tag{6.39}$$

In which the $\tilde{\rho}_{L,MP}$ is the interpolated liquid density field. Using this procedure, the interpolated density $\tilde{\rho}_{L,MP}$ is evaluated for all material points, which is used in the current MPM formulation to capture the free surface; i.e.

$$\tilde{\rho}_{L,MP} \leq F_{FreeSurf}\, \rho_{L,0} \tag{6.40}$$

where $\rho_{L,0}$ is the reference value of the liquid density described in Section 7.2.1 and $F_{FreeSurf}$ is the factor that controls the continuity of the free surface. The bigger is this value, but always smaller than 1, the greater is the number of particles detected. This factor is mesh dependence and needs to be set accordingly. The value suggested for this factor is 0.7.

# 7 Constitutive models

This chapter presents the fundamental theories in constitutive modelling for solids applied to soils and to fluids.

## 7.1 Constitutive models for solids

The constitutive models is a small part in the code, which converts the strain increments into stress increments and defines the stiffness of the material. It plays two fundamental roles in large deformation MPM simulations [25, 26].

1 It controls the failure at small deformation as in finite element (FE) simulations.
2 It controls the dissipation of energy and, hence, it dictates the post-failure behaviour.

In the past years, a plethora of constitutive models have been suggested. Each one of them was developed for specific conditions and makes its own assumptions. Therefore, the choice of the constitutive model depends on the type of soils and the problem to be modelled, and relies on the engineering judgement of the modeller. It is important to insure that the chosen model is able to capture the mechanics of interests as it will have significant impact on the computational time and the simulation results.

Although the numerical methods do change from one field of engineering to another, constitutive models do. For instance, compression is usually taken in geomechanics as positive in compression and negative in tension, whilst this is not the case in mechanical engineering. This means that the sign convention within the constitutive model is often inverted inside the constitutive model, and then reverted when giving the information back to the kernel of the code. Moreover, the mechanical behaviour of soil is known to be history-dependent and history state variables are used in many models. This history-dependency can only be tracked in numerical methods formulated in the weak form (i.e. FE) and is one of the main reason MPM is interesting for geotechnical engineering.

The development of constitutive model, or stress-strain relationships, has been in the light of research ever since the early days of soil mechanics, and there has been many significant changes throughout time. Two big families of models exists – those developed from failure criteria and those develop from energy consideration. Historically, the first type of models to have emerged were from failure criteria. These are empirical formula which predict the stress state at failure without considering the strain state (i.e. Mohr-Coulomb, Tresca). They were then combined with elasticity in order to get a first estimate of the strain state and, later, further developed to include plastic deformation. These models are often referred to as *elastic-plastic* models as the hardening phase is solely elastic. The second type of models emerged from the work of Roscoe and Schofield [27–30], who developed a stress-strain framework based on energy dissipation, also known as the Critical State Soil Mechanics framework [31]. These models are often referred to as *elasto-plastic models* as the hardening phase includes plasticity. Both types of model are depicted in this chapter.

A major difference with standard FE is that MPM can model large deformations. However, this implies that large deformation stresses have to be taken into account. Many constitutive equations are designed in the form of a relation between a stress rate and a strain rate (or the rate of deformation tensor). The principle of material objectivity or material frame indifference states that the material response is independent of the observer, and different forms of ob-

jective stress rate can be found in continuum mechanics [32]. Anura3D adopts the Jaumann stress rate which writes the material time derivative of the Cauchy stress tensor as follows

$$\hat{\boldsymbol{\sigma}}^{\nabla \mathrm{J}} = \mathrm{d}\boldsymbol{\sigma} - \mathbf{W} \cdot \boldsymbol{\sigma} + \boldsymbol{\sigma} \cdot \mathbf{W}^{\mathbf{T}} \tag{7.1}$$

Eq. 7.1 shows three terms. The first one is the rate of change due to the material response; the other two terms represent the change of stress due to rotation. The term **W** is the skew part of the velocity gradient tensor that can be written as

$$\mathrm{W_{ij}} = \frac{1}{2}\left(\frac{\partial \mathrm{v_i}}{\partial \mathrm{x_j}} - \frac{\partial \mathrm{v_j}}{\partial \mathrm{x_i}}\right) \tag{7.2}$$

### 7.1.1 General formulation

The stress-strain relationship of soil is non-linear and incremental. It follows the principle of effective stresses [33], which states than any changes in the effective stresses will result in changes in strains, and vice versa. The effective stress increment $\mathrm{d}\vec{\sigma}'$ is related to the strain increment $\mathrm{d}\vec{\varepsilon}$ by the stiffness matrix **D**, which is determined by the constitutive model. The incremental stress-strain equation can be written as shown in Eq. 7.3.

$$\mathrm{d}\vec{\sigma}' = \mathbf{D} \cdot \mathrm{d}\vec{\varepsilon} \tag{7.3}$$

The strains are decomposed into recoverable elastic and irrecoverable plastic strains (Eq. 7.4).

$$\mathrm{d}\vec{\varepsilon} = \mathrm{d}\vec{\varepsilon}^{\mathrm{e}} + \mathrm{d}\vec{\varepsilon}^{\mathrm{p}} \tag{7.4}$$

where $\mathrm{d}\vec{\varepsilon}^{\mathrm{e}}$ and $\mathrm{d}\vec{\varepsilon}^{\mathrm{p}}$ are the elastic and plastic strain increments, respectively.

The elastic stress-strain is expressed by Hooke's law [34]. The elastic strain increment $\mathrm{d}\vec{\varepsilon}^{\mathrm{e}}$ can be formulated in terms of the total strain increments $\mathrm{d}\vec{\varepsilon}$ and the plastic strain increment $\mathrm{d}\vec{\varepsilon}^{\mathrm{p}}$ (Eq. 7.5).

$$\mathrm{d}\vec{\sigma}' = \mathbf{D_e} \cdot \mathrm{d}\vec{\varepsilon}^{\mathrm{e}} \quad \rightarrow \quad \mathrm{d}\vec{\sigma}' = \mathbf{D_e} \cdot (\mathrm{d}\vec{\varepsilon} - \mathrm{d}\vec{\varepsilon}^{\mathrm{p}}) \tag{7.5}$$

where $\mathbf{D_e}$ is the elastic stiffness matrix.

#### 7.1.1.1 Elasticity

The elastic behaviour of soil is characterised by reversible deformation. Elasticity is defined by any two elastic parameters, which can be E the Young's modulus, $\nu$ the Poisson ratio, K the bulk modulus, G the shear modulus, $\kappa$ the swelling modulus, etc. The formulation of the work equation with the Cambridge stress invariants $(\mathrm{p}', \mathrm{q})$ requires the definition the bulk modulus K and the shear modulus G. Therefore, the incremental equation can be formulated as shown in Eqs. 7.6 and 7.7.

$$\mathrm{dp}' = \mathrm{K} \cdot \mathrm{d}\varepsilon_{\mathrm{v}}^{\mathrm{e}} \tag{7.6}$$

$$\mathrm{dq}' = 3\mathrm{G} \cdot \mathrm{d}\varepsilon_{\mathrm{d}}^{\mathrm{e}} \tag{7.7}$$

where K is the bulk modulus and G the shear modulus.

The Poisson ratio $\nu$ is often assumed to be a constant with a value of 0.2 [35]. It defines the first elastic parameter. The second elastic parameter is a matter of choice. It is customary to determine the shear modulus G for sand and to then calculate the bulk modulus K (Eqs. 7.8 and 7.9)

$$G = A\left(\frac{p'}{p_{ref}}\right)^{n} \tag{7.8}$$

$$K = \frac{2}{3}\frac{1+\nu}{1-2\nu}\cdot G \tag{7.9}$$

where A is the shear modulus constant, $p_{ref}$ the unit reference pressure, $n^e$ the shear modulus exponent and $\nu$ the Poisson ratio, which is denoted with the Greek letter 'nu'.

However, it is customary to do the opposite for clay – calculate the bulk modulus K and then them convert it to a shear modulus G.

$$K = \frac{vp'}{\kappa} \tag{7.10}$$

$$G = \frac{3K(1-2\nu)}{(2+2\nu)} \tag{7.11}$$

where $v = 1 + e$ is the specific volume and denoted with the Roman letter 'v' and $\kappa$ is the Swelling modulus; these will be further discussed in this chapter.

The elastic stiffness matrix $\mathbf{D}^e$ using the bulk modulus K and the shear modulus G can be written as Eq. 7.12 .

$$\mathbf{D}^e = \begin{bmatrix} K+\frac{4}{3}G & K-\frac{2}{3}G & K-\frac{2}{3}G & 0 & 0 & 0 \\ K-\frac{2}{3}G & K+\frac{4}{3}G & K-\frac{2}{3}G & 0 & 0 & 0 \\ K-\frac{2}{3}G & K-\frac{2}{3}G & K+\frac{4}{3}G & 0 & 0 & 0 \\ 0 & 0 & 0 & G & 0 & 0 \\ 0 & 0 & 0 & 0 & G & 0 \\ 0 & 0 & 0 & 0 & 0 & G \end{bmatrix} \tag{7.12}$$

However, the elastic stiffness matrix $\mathbf{D}^e$ can equivalently be built from the Young's modulus E and the Poisson ratio $\nu$ as shown in Eq. 7.13.

$$\mathbf{D^e} = \frac{E}{(1-2\nu)(1+\nu)}\begin{bmatrix} 1-\nu & \nu & \nu & 0 & 0 & 0 \\ \nu & 1-\nu & \nu & 0 & 0 & 0 \\ \nu & \nu & 1-\nu & 0 & 0 & 0 \\ 0 & 0 & 0 & \frac{1}{2}-\nu & 0 & 0 \\ 0 & 0 & 0 & 0 & \frac{1}{2}-\nu & 0 \\ 0 & 0 & 0 & 0 & 0 & \frac{1}{2}-\nu \end{bmatrix} \tag{7.13}$$

The way the elastic stiffness matrix $\mathbf{D}^e$ is built is model dependent.

#### 7.1.1.2 Plasticity

***The yield function*** is a function used to identify if the soil will undergo some plastic deformation. The plastic behaviour of soil is characterised by its irrecoverable deformations. It is mainly caused by the displacement and the rearrangement of the soil grains. Taylor [36] showed that the development of strength was associated with the changes in volume and that it was as a consequence of grains interlocking and inter-granular friction. [28] were driven by this idea and expressed Taylor's stress-dilatancy as stress invariants (Eq.7.14).

$$p'd\varepsilon_v^p + qd\varepsilon_d^p = p'Md\varepsilon_d^p \tag{7.14}$$

The rearrangement of the terms gives a stress-dilatancy rule in terms of stress invariants (Eq. 7.15), and can be used as a flow rule. This new formulation of the stress-dilatancy relationship expresses the strength $\eta'$ as a consequence of friction M and interlocking D.

$$\rightarrow \eta' = M - D \tag{7.15}$$

where $\eta' = q/p'$ is the effective stress ratio, M the critical state effective stress ratio and $D = d\varepsilon_d/d\varepsilon_v$ the dilatancy rate.

Roscoe et al. [28] then followed the work of Drucker et al. [37] and the stress-dilatancy flow rule (Eq. 7.15) becomes a differential equation (Eq. 7.16).

$$D = -\frac{\partial q}{\partial p'} \rightarrow \eta = M + \frac{\partial q}{\partial p'}$$

$$q = \eta' \cdot p' \rightarrow \eta' = M + \frac{\partial(\eta' p')}{\partial p'} \rightarrow \eta' = M + \frac{\partial \eta'}{\partial p'} p' + \eta'$$

$$\frac{\partial p'}{p'} = -\frac{\partial \eta'}{M} \tag{7.16}$$

A unique solution can be found and the constant determined by formulating the initial stress state ($q = 0$, $p' = p'_0$, $\eta' = 0$). The initial pressure $p'_0$ will be called later the consolidation pressure $p_c$. Therefore, the integration of the differential equation (Eq. 7.16) gives to Eq. 7.17.

$$\rightarrow F = \eta' - M \ln\left(\frac{p_c}{p'}\right) \leq 0 \tag{7.17}$$

where F is the yield function of Original Cam-Clay [28], which was the first elasto-plastic model to be developed.

***The potential function*** P defines the direction of the strain increments and can differ from the yield function F. The relationship between the stress and strain increments is called the *flow rule* and is shown in (Eq. 7.18).

$$d\vec{\varepsilon}_p = \Lambda \frac{\partial P}{\partial \vec{\sigma'}} \tag{7.18}$$

where P is the potential function and $\Lambda$ the hardening term, which is denoted by a capital letter to avoid confusion with the critical state slope $\lambda$.

The model is said to be *associative* when the stress and strain increments are coaxial and, hence, the yield and potential functions are equal (P = F). The model is said to be *non-associative* when the stress and strain increments are not coaxial (P $\neq$ F).

The inclusion of the flow rule in the incremental stress-strain equation (Eq. 7.5) gives Eq. 7.19.

$$d\vec{\sigma'} = \mathbf{D_e}\left(d\vec{\varepsilon} - \Lambda\frac{\partial P}{\partial\vec{\sigma'}}\right) \tag{7.19}$$

where $\Lambda$ is the hardening term.

The plastic multiplier $\Lambda$ can be determined by introducing the conditions given in Eq. 7.20.

$$F \leq 0 \tag{7.20a}$$
$$\Lambda \geq 0 \tag{7.20b}$$
$$F\Lambda = 0 \tag{7.20c}$$

which help distinguishing between plastic and elastic loading and unloading.

F = 0 and $\Lambda > 0$ indicate plastic conditions; F < 0 with $\Lambda = 0$ represents the elastic conditions. F = d$\Lambda$ = 0 is called neutral loading. These conditions must be fulfilled at all times. This implies that the increase of stresses during plastic flow relates to the increase of the hardening parameters such that the stresses remain on the yield surface. In other words, F + dF = 0, and with F = 0 this implies that dF = 0 during plastic flow. This is called the consistency condition.

***The consistency condition*** says that the total derivative of the yield function must be nil. The yield function is a function of stresses and strains and its derivative gives Eq. 7.21.

$$dF = \frac{\partial F}{\partial\sigma'}d\vec{\sigma'} + \frac{\partial F}{\partial\varepsilon^p}d\vec{\varepsilon}_p = 0 \tag{7.21}$$

The development of the consistency condition (Eq. 7.21) with the flow rule and the incremental stress-strain equation (Eq. 7.19) gives Eq. 7.22.

$$\rightarrow d\vec{\sigma'} = \mathbf{D_e}\left[1 - \frac{\left(\frac{\partial F}{\partial\vec{\sigma'}}\right)^t \mathbf{D_e}\frac{\partial P}{\partial\vec{\sigma'}}}{\left(\frac{\partial F}{\partial\vec{\sigma'}}\right)^t \mathbf{D_e}\frac{\partial P}{\partial\vec{\sigma'}} - \left(\frac{\partial F}{\partial\vec{\varepsilon^p}}\right)^t \frac{\partial P}{\partial\vec{\sigma'}}}\right] d\vec{\varepsilon} \tag{7.22}$$

***The hardening rule*** $\partial F/\partial\vec{\varepsilon^p}$ controls the hardening and the softening, and thus the size of the yield surface. It is also the term in which the critical state conditions is embedded (D = $\partial D/\partial\varepsilon_d$ = 0).

The hardening rule is a function of the plastic work and can be written as shown in Eq. 7.23. The actual expression of the terms depends on the assumptions of the model.

$$\frac{\partial F}{\partial\vec{\varepsilon^p}} = \frac{\partial F}{\partial W^p}\frac{\partial W^p}{\partial\vec{\varepsilon^p}} \tag{7.23}$$

where $W^p$ is the plastic work.

Therefore, the stiffness of the soil is a imposed by the yield function, the potential function and the hardening rule.

### 7.1.2 Elastic-plastic models

Elastic-plastic models assume that the soil hardens with elastic deformation until a threshold is reached (F = 0). These are often the extension of failure criteria to stress-strain relationships, and were often originally for steel (i.e. Tresca [38], von Misses [39], Mohr [40], etc.), but have been used to model solids including soils.

#### 7.1.2.1 Tresca

Tresca [38] observed that the failure of solids occurs at a given shear stress and, subsequently, wrote a yield criterion which is expressed in principal stress in Eq. 7.24.

$$F_1 = \frac{|\sigma'_2 - \sigma'_3|}{2} - \tau_f \tag{7.24a}$$

$$F_2 = \frac{|\sigma'_1 - \sigma'_3|}{2} - \tau_f \tag{7.24b}$$

$$F_3 = \frac{|\sigma'_1 - \sigma'_2|}{2} - \tau_f \tag{7.24c}$$

where F is the yield function, $\sigma'$ is the effective stress, $\tau_f$ the shear stress at failure and the subscripts refer to the principal stresses.

The yield surface of the Tresca model forms hexagonal prism in the principal stress space, as shown in Fig. 7.1.

An associative flow rule is typical used in the model, i.e. the plastic potential coincide with the yielding function. The model is elastic-perfectly plastic, i.e. the yielding function does not change during plastic deformations, therefore no hardening law needs to be specified. The isotropic linear elastic law is used within this constitutive model.

The Tresca model is typically used in geotechnical engineering to model the undrained strength of clayey soils, in which case $\tau_f = s_u$ with $s_u$ being the undrained shear strength. The Tresca model is a simplified model of Mohr-Coulomb [33], which will be discussed in the next section, in which the friction and dilatancy angles are nil ($\varphi = 0$, $\psi = 0$) and the cohesion is equal to the shear strength ($c = s_u$).

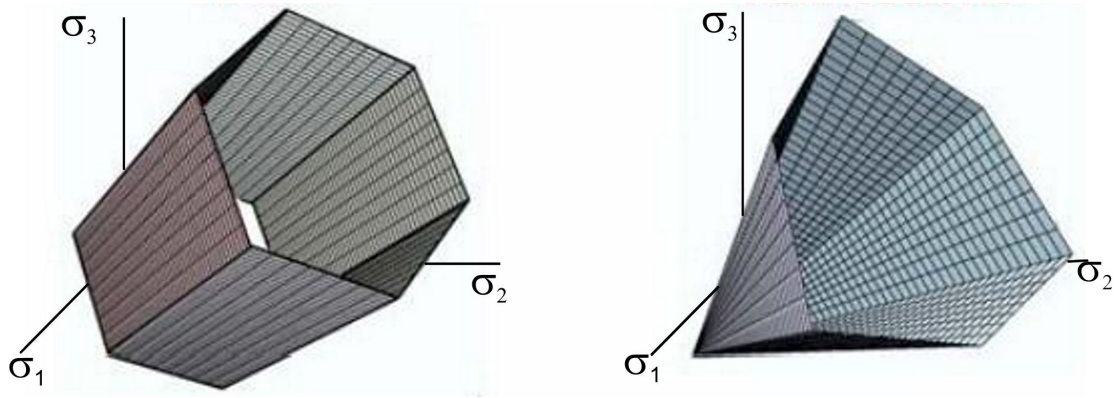


***Figure 7.1:*** *Tresca (left) and Mohr-Coulomb (right) failure surfaces (compression is positive).*

#### 7.1.2.2 Mohr-Coulomb

Terzaghi [33] investigated the behaviour of soil with the direct shear apparatus and observed that the shear strength of soil was stress dependent. He then developed a failure criterion based on the the work of Mohr [40] on brittle steel and work of Coulomb [41] on friction. He subsequently named the yield criterion 'Mohr-Coulomb'. The failure criteria is based on a stress-dependent term with the friction angle $\varphi'$ as a model parameter, and an intercept value defined as the cohesion c′

$$\tau_f = c' + \sigma'_N \tan(\varphi') \tag{7.25}$$

where c′ is the cohesion, $\sigma'_N$ the stress normal to the shear plane and $\varphi'$ the friction angle.

The Mohr-Coulomb failure criteria can be formulated in terms of yield function and in the principal stress space as shown in Eq. 7.26.

$$F_1 = \frac{|\sigma'_2 - \sigma'_3|}{2} + \frac{\sigma'_2 + \sigma'_3}{2} \sin(\varphi') - c' \cos(\varphi') \tag{7.26a}$$

$$F_2 = \frac{|\sigma'_1 - \sigma'_3|}{2} + \frac{\sigma'_1 + \sigma'_3}{2} \sin(\varphi') - c' \cos(\varphi') \tag{7.26b}$$

$$F_3 = \frac{|\sigma'_1 - \sigma'_2|}{2} + \frac{\sigma'_1 + \sigma'_2}{2} \sin(\varphi') - c' \cos(\varphi') \tag{7.26c}$$

Fig. 7.1 shows the yield function in the generalised stress space and forms an hexagonal cone. The main difference between a Tresca criterion and a Mohr-Coulomb criterion is the pressure-dependency, which transforms the prism into a cone.

The transformation of the Mohr-Coulomb failure criterion into a constitutive model requires defining a plastic potential function P (Eq. 7.27) and the introduction of a third model parameter - the dilatancy angle $\psi$ .

$$P_1 = \frac{|\sigma'_2 - \sigma'_3|}{2} + \frac{\sigma'_2 + \sigma'_3}{2} \sin(\psi) \tag{7.27a}$$

$$P_2 = \frac{|\sigma'_1 - \sigma'_3|}{2} + \frac{\sigma'_1 + \sigma'_3}{2} \sin(\psi) \tag{7.27b}$$

$$P_3 = \frac{|\sigma'_1 - \sigma'_2|}{2} + \frac{\sigma'_1 + \sigma'_2}{2} \sin(\psi) \tag{7.27c}$$

Therefore, Mohr-Coulomb models the hardening phase, or increase in strength, as elastic until it reaches the failure criterion defined by c′ and $\varphi'$, in which state it flows at a constant strength (perfectly plastically). The strains are elastic during the hardening phase, and hence the soil contracts, until the failure criterion is reached. At which point, the plastic volume changes are governed by the dilatancy angle $\psi$. Unlike Cambridge type of model presented later in this chapter, there is no direct correlation between the strength and the strains built into the model. Therefore, it is the duty of the modeller to insure mechanical consistency.

There has been extensive discussion during the 1950s and 1960s on what is the friction angle of soils as it is pressure and state dependent, and what is the meaning of the model parameters c′ and $\varphi'$ as they can equally be applied to the peak strength and the critical (residual) strength. Historically, the peak strength was considered as the failure point and Bishop [42] argued that the cohesion c′ would relate to the dilatancy angle $\psi$. However,

Roscoe et al. [27] argued that cohesion is nil ($c' = 0$) and that it is the friction angle which relates to both the critical state friction angle $\varphi_{cs}$ and the dilatancy $\psi$ (Eq. 7.28) [43].

$$\varphi' = \varphi'_{cs} + 0.8\psi \tag{7.28}$$

## 7.2 Constitutive models for liquids

### 7.2.1 Newtonian fluid

For weakly compressible liquids, the density of the constituent is related to the liquid pressure as follows

$$\frac{\partial \rho_L}{\partial t} = -\frac{1}{c_p^2}\frac{\partial p_L}{\partial t} \; ; \; c_p = \sqrt{K_L/\rho_L} \tag{7.29}$$

where $c_p$ is the acoustic wave speed with $K_L$ being the elastic modulus of the liquid. For relatively small range of pressure and during isothermal process, $c_p$ is a constant value and the pressure-density relation becomes linear, as shown in Fig. 7.2:

$$p_L = p_{L,0} - c_p^2(\rho_L - \rho_{L,0}) \tag{7.30}$$

where $p_{L,0}$ and $\rho_{L,0}$ are the reference values for pressure and density, which are set respectively to 0kPa and 1Mg/m$^3$, and $c_p = \sqrt{K_L/\rho_{L,0}}$.

The value of liquid pressure at which the cavitation occurs is $p_{L,thres}$ and the corresponding density is $\rho_{L,thres}$ that can be determined as

$$\rho_{L,thres} = \frac{1}{c_p^2}(p_{L,0} - p_{L,thres}) + \rho_{L,0} = \rho_{L,0}(1 - \frac{p_{L,thres}}{K_L}) \tag{7.31}$$

In case of $\rho_L \geq \rho_{L,thres}$, the pressure can be directly calculated as function of the volumetric strain $\varepsilon_{vol,L}$ as follows

$$p_L = p_{L,thres} + K_L\varepsilon_{vol,L} \tag{7.32}$$

Conversely, the pressure is set to $p_{L,thres}$.

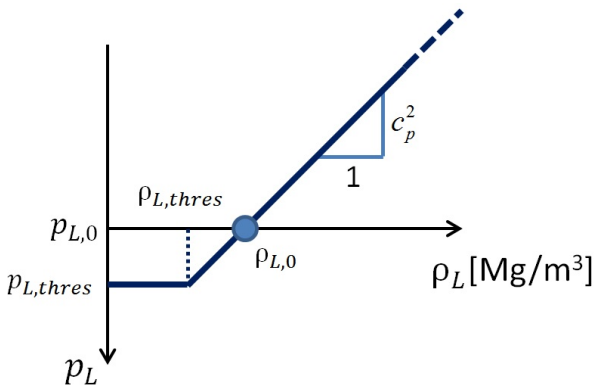


***Figure 7.2:*** *Constitutive behaviour of compressible liquid.*

In the current study, the pressure in the liquid constituent is computed in the incremental form as follows:

$$\frac{dp_L}{dt} = K_L \frac{d\bar{\varepsilon}_{vol,L}}{dt} \quad \text{with} \quad p_L \geq p_{L,thres} \tag{7.33}$$

(7.34)

In case of 2-phase-coupled, the term $\frac{d^L\bar{\varepsilon}_{vol,L}}{dt}$ is calculated according to the mass balance equation as Eq. 3.23, and repeated hereafter. In case of 1-phase-liquid, the term $\bar{\varepsilon}$ is equal to the volumetric strain of the liquid material ($\bar{\varepsilon}_{vol,L} = \varepsilon_{vol,L}$).

$$\frac{d^L\bar{\varepsilon}_{vol,L}}{dt} = \frac{1}{n}[n(\nabla \cdot \mathbf{v}_L) + (1-n)(\nabla \cdot \mathbf{v}_S)] \tag{7.35}$$

Lastly, the deviatoric part of the stress tensor is calculated as

$$\boldsymbol{\sigma}_{dev,L} = 2\mu_d \frac{D^L\varepsilon_{dev,L}}{Dt} \quad \text{with} \quad p_L > p_{L,thres} \tag{7.36}$$

where $\mu_d$ is the dynamic viscosity of the water, and $\varepsilon_{dev,L}$ is the deviatoric part of the strain tensor. Eq. (7.36) is used only in case of pure liquid (1-phase-liquid). In case of 2-phase-coupled, the shear stresses in the liquid part vanish.

### 7.2.2 Bingham fluid

A Bingham fluid is a visco-plastic material that behaves as an elastic body at low shear stresses but flows as a viscous fluid at high shear stress. An example is toothpaste, which will not be extruded until a certain pressure is applied to the tube, then it is pushed out as a solid plug. It has been used as a constitutive model to simulate a number of geophysical flows, such as mud flow, snow avalanches, debris flow, drilling slurry, and concrete [44].

Contrary to solid mechanicians, for whom plasticity means loss of reversibility in material deformations, fluid rheologists have related plasticity to solid/fluid transition: the yield stress of a solid would be the stress at which the solid first starts to deform continuously, i.e. to flow. In this perspective, the yield stress marks the limit between solid-like (assumed to be elastic) and fluid-like (viscous) behaviours.

The stress increment is computed with a linear elastic law until the shear stress remains lower than the yield stress $\tau_y$. Beyond this shear stress level the material behaves as a viscous fluid. In yielding conditions, the stress of the fluid is computed like in Newtonian fluid, as explained in Section 7.2.1, but an effective viscosity $\mu_{eff}$ , which takes into account of the contribute of $\tau_y$, is used in place of the dynamic viscosity.

The effective viscosity is computed as:

$$\mu_{eff} = \begin{cases} \frac{\mu_d + \tau_y}{\|\mathbf{D}\|} & \text{for} \quad \mu_{eff} < \mu_{max} \\ \mu_{max} & \text{for} \quad \mu_{eff} \leq \mu_{max} \end{cases} \tag{7.37}$$

where $\|\mathbf{D}\|$ is the norm of the deviatoric strain rate tensor; and $\mu_{max}$ is a bound for the effective viscosity that prevents the occurrence of very large values of viscosity when the shear rate goes to zero.

In summary, the material input parameters are:

- ◇ the Young's modulus E and the Poisson's ratio $\nu$, which are used until the shear stress is lower than the yield stress;
- ◇ the yield stress $\tau_y$, which defines the boundary between linear-elastic and visco-plastic behaviour;
- ◇ the bulk modulus of the fluid K, which is used to compute the pressure increment;
- ◇ the dynamic viscosity $\mu_d$, which relates the shear rate and the shear stress.

### 7.2.3 Frictional fluid

Most of geophysical flows involves granular materials, such as soil. These materials behave like solids until a limit condition is reached and like viscous fluids when the flow initiates. The boundary condition between the solid-like and the liquid-like behaviour is pressure-dependent and it is usually represented with a Mohr-Columb or Drucker-Prager criterion.

The constitutive model described in this Section is very similar to the Bingham fluid model introduced in Section 7.2.2, but here the yield stress $\tau_y$ is a function of the fluid pressure through a friction angle according to the Drucker-Prager condition:

$$\tau_y = p \sin \phi \tag{7.38}$$

The material input parameters are:

- ◇ the friction angle $\phi$, which define the boundary between linear-elastic and visco-plastic behaviour;
- ◇ the Young's modulus E and the Poisson's ratio $\nu$, which are used until the shear stress is lower than the yield stress;
- ◇ the bulk modulus of the fluid K, which is used to compute the pressure increment;
- ◇ the dynamic viscosity $\mu_d$, which relates the shear rate and the shear stress.

## References


[1] Francis H Harlow. The particle-in-cell computing method for fluid dynamics. *Methods in computational physics*, 3(3):319–343, 1964.

[2] Deborah Sulsky, Z. Chen, and H.L. Schreyer. A particle method for hystory-dependent materials. *Computer Methods in Applied Mechanics and Engineering*, 118(1-2):179–196, 1994.

[3] Deborah Sulsky, Shi-Jian Zhou, and Howard L. Schreyer. Application of a particle-in-cell method to solid mechanics. *Computer Physics Communications*, 87(1-2):236–252, May 1995. ISSN 00104655. doi: 10.1016/0010-4655(94)00170-7. URL http://linkinghub.elsevier.com/retrieve/pii/0010465594001707.

[4] D Sulsky and HL Schreyer. Axisymmetric form of the material point method with applications to upsetting and Taylor impact problems. *Computer Methods in Applied Mechanics and Engineering*, 0457825(96), 1996. URL http://www.sciencedirect.com/science/article/pii/S0045782596010912.

[5] A. Yerro. *MPM modelling of landslides in brittle and unsaturated soils*. PhD Thesis, Universitat Politècnica de Catalunya (UPC Barcelona), Spain, 2015.

[6] OC Zienkiewicz and T Shiomi. Dynamic behaviour of saturated porous media; the generalized Biot formulation and its numerical solution. *International Journal for Numerical and Analytical Methods in Geomechanicsnumerical and analytical methods . . .*, 8:71–93, 1984. URL http://onlinelibrary.wiley.com/doi/10.1002/nag.1610080106/abstract.

[7] O. C. Zienkiewicz, a. H. C. Chan, M. Pastor, D. K. Paul, and T. Shiomi. Static and Dynamic Behaviour of Soils: A Rational Approach to Quantitative Solutions. I. Fully Saturated Problems. *Proceedings of the Royal Society A: Mathematical, Physical and Engineering Sciences*, 429(1877):285–309, June 1990. ISSN 1364-5021. doi: 10.1098/rspa.1990.0061. URL http://rspa.royalsocietypublishing.org/cgi/doi/10.1098/rspa.1990.0061.

[8] Olgierd C Zienkiewicz, AHC Chan, M Pastor, BA Schrefler, and T Shiomi. *Computational geomechanics*. Wiley Chichester, 1999.

[9] J Van Esch, Dieter Stolle, Issam Jassim, and J M van Esch. Finite element method for coupled dynamic flow-deformation simulation. *2nd International Symposium on . . .*, (1), 2011. URL http://www.uni-stuttgart.de/igs/content/publications/218_Issam_Dubrovnik.pdfhttp://www.researchgate.net/publication/259579508_FINITE_ELEMENT_METHOD_FOR_COUPLED_DYNAMIC_FLOW-DEFORMATION_SIMULATION/file/e0b4952cbd16168e83.pdf.

[10] I.K.J. Al-Kafaji. *Formulation of a dynamic material point method (MPM) for geomechanical problems*. PhD Thesis, Institut für Geotechnik der Universität Stuttgart, Germany, 2013.

[11] Jeremiah U Brackbill, Douglas B Kothe, and Hans M Ruppel. Flip: A low-dissipation, particle-in-cell method for fluid flow. *Computer Physics Communications*, 48(1):25–38, 1988.

[12] P. A. Vermeer. *PLAXIS 2D Reference Manual Version 5*. Balkema, Rotterdam / Brookfield, 1993.

[13] M.M.J. Mieremet. Numerical stability for velocity-based 2-phase formulation for geotechnical dynamic analysis. Report 15-03, ISSN 1389-6520, Reports of the Delft Institute of Applied Mathematics, Delft University of Technology, Delft, The Netherlands, 2015.

[14] M.M.J. Mieremet. *Numerical stability for velocity-based 2-phase formulation for geotechnical dynamic analysis*. MSc Thesis, Applied Mathematics, Delft University of Technology, Delft, The Netherlands, 2015.

[15] E. Alonso and F. Zabala. Progressive failure of Aznalcóllar dam using the material point method. *Géotechnique*, 61(9):795–808, 2011. doi: 10.1680/geot.9.P.134.

[16] E. Love and D.L. Sulsky. An unconditionally stable, energy–momentum consistent implementation of the material-point method. *Computer Methods in Applied Mechanics and Engineering*, 195(33-36):3903–3925, July 2006. ISSN 00457825. doi: 10.1016/j.cma.2005.06.027. URL http://linkinghub.elsevier.com/retrieve/pii/S0045782505003592.

[17] S.G. Bardenhagen, J.E. Guilkey, K.M. Roessig, J.U. Brackbill, W.M. Witzel, and J.C. Foster. An improved contact algorithm for the material point method and application to stress propagation in granular material. *Computer Modeling in Engineering and Sciences*, 2: 509–522, 2001.

[18] Andrew Gemant and Willis Jackson. Xciii. the measurement of internal friction in some solid dielectric materials. *The London, Edinburgh, and Dublin Philosophical Magazine and Journal of Science*, 23(157):960–983, 1937.

[19] RL Wegel and H Walther. Internal dissipation in solids for small cyclic strains. *Journal of Applied Physics*, 6(4):141–157, 1935.

[20] PA Cundall. *FLAC Manual: A Computer Program for Fast Lagrangian Analysis of Continua*, 2001.

[21] R Hart, PA Cundall, and J Lemos. Formulation of a three-dimensional distinct element model: Part ii. mechanical calculations for motion and interaction of a system composed of many polyhedral blocks. In *International Journal of Rock Mechanics and Mining Sciences & Geomechanics Abstracts*, volume 25, pages 117–125. Elsevier, 1988.

[22] PA Cundall. Distinct element models of rock and soil structure. *Analytical and computational methods in engineering rock mechanics*, 4:129–163, 1987.

[23] C.M. Mast, P. Mackenzie-Helnwein, P. Arduino, G.R. Miller, and W. Shin. Mitigating kinematic locking in the material point method. *Journal of Computational Physics*, 231 (16):5351–5373, June 2012. ISSN 00219991. doi: 10.1016/j.jcp.2012.04.032. URL http://linkinghub.elsevier.com/retrieve/pii/S0021999112002148.

[24] C Detournay and E Dzik. Nodal mixed discretization for tetrahedral elements. In *4th international FLAC symposium, numerical modeling in geomechanics. Minnesota Itasca Consulting Group, Inc. Paper*, number 07-02, 2006.

[25] E.J. Fern and K. Soga. The role of constitutive models in MPM simulations of granular column collapses. *Acta Geotechnica*, 11(3):659–678, 2016. doi: 10.1007/s11440-016-0436-x.

[26] E.J. Fern. *Constitutive modelling of unsaturated sand and its application to large deformation modelling*. PhD thesis, University of Cambridge, 2016.

[27] K.H. Roscoe, A. N. Schofield, and C. P. Wroth. On the yielding of soil. *Géotechnique*, 8: 22–52, 1958. doi: 10.1680/geot.1958.8.1.22.

[28] K.H. Roscoe and A. N. Schofield. Mechanical behaviour of an idealised wet clay. In *2nd European Conference on Soil Mechanics and Foundation Engineering*, pages 47–54, Wiesbaden, 1963.

[29] K.H. Roscoe and J.B. Burland. *Engineloads plasticity*, chapter On generalised stress strain behaviour of wet clay, pages 535–609. 1968.

[30] K.H. Roscoe. The Influence of strains in soil mechanics. *Géotechnique*, 20(2):129–170, 1970. doi: 10.1680/geot.1970.20.2.129.

[31] Andrew Schofield and Peter Wroth. *Critical state soil mechanics*. McGraw-Hill London, 1968.

[32] Ted Belytschko, Wing Kam Liu, Brian Moran, and Khalil Elkhodary. *Nonlinear finite elements for continua and structures*. John Wiley & Sons, second edition, 2013.

[33] K. Terzaghi. *Theoretical Soil Mechanics*. John Wiley & Sons, Inc., New York, first edition, 1943. doi: 10.1680/geot.1964.14.1.1.

[34] R. Hooke. *De Potentia Restitutiva, or of Spring*. J. Martyn, London, 1678.

[35] Michael Jefferies and Ken Been. *Soil liquefaction: a critical state approach*. CRC Press, 2006.

[36] D.W. Taylor. *Fundamental of Soil Mechanics*. John Wiley & Sons, New York, 1948.

[37] D.C. Drucker, R.E. Gibson, and D.J. Henkel. Soil mechanics and work-hardening theories of plasticity. *Journal of Soil Mechanics and Foundation Engineering1*, 122:338–346, 1957.

[38] H. Tresca. Mémoire sur l'écoulement des corps solides soumis à de fortes pressions. *Rendus hebdomadaires des séances de l'Académie des Sciences*, 59:754–758, 1864.

[39] R. von Mises. Mechanik der festen Körper im plastisch-deformablen Zustand, Nachrichten von der Gesellschaft der Wissenschaften zu Göttingen. *Mathematisch-Physikalische Klasse 1*, pages 582–592, 1913.

[40] C.O. Mohr. *Welche Umstaad Bedingen des Elastizitaetsgrenzen und den Bruch eines material? Abhandlingen aus dem Gebiete der Technischen Mechanik*. Ernst und Sohn, Berlin, 3rd edition, 1928.

[41] C.A. Coulomb. *Essai sur une application des règles de maximis & minimis à quelques problèmes de statique relatif à l'architecture*. De l'Imprimerie Royale, 1776.

[42] A.W. Bishop. Discussion: Shear characteristics of a saturated silt, measured in triaxial compression. *Géotechnique*, 43(1):43–45, 1954.

[43] MD Bolton. The strength and dilatancy of sands. *Geotechnique*, 36(1):65–78, 1986.

[44] Christophe Ancey. Plasticity and geophysical flows: a review. *Journal of Non-Newtonian Fluid Mechanics*, 142(1):4–35, 2007.